Progress in Natural Science: Materials International 34 (2024) 74–88

HOSTED BY

Contents lists available at ScienceDirect

Progress in Natural Science: Materials International

journal homepage: www.elsevier.com/locate/pnsmi

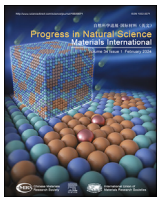

Electronic nose based on metal oxide semiconductor sensors for medical diagnosis

Zicong Zhang, Zichen Zheng, Xiaoxi He, Kewei Liu, Marc Debliquy, Yiwen Zhou, Chao Zhang *

College of Mechanical Engineering, Yangzhou University, Yangzhou, 225009, PR China

ARTICLE INFO

Keywords:
Metal oxide semiconductor
Sensing materials
Medical diagnosis
Volatile organic compounds

ABSTRACT

As malignant diseases are responsible for high mortality rates invariably, there is presently a pressing need to develop innovative medical diagnostic techniques due to the limitations of current approaches, including non-invasiveness, inability to monitor real-time, and the associated high cost of the equipment. Specifically, breath analysis has received a great deal of attention over the past two decades. Volatile organic compounds (VOCs) in exhaled breath could reflect the metabolic and physiological processes of the human body. Thus the electronic nose (E-nose) which comprises an array of gas sensors, signal acquisition, a pre-processing unit, and a pattern recognition algorithm that mimics the human sense of smell, can diagnose illnesses by analyzing exhaled breath fingerprints accurately, showing their irreplaceable features of non-invasive, real-time monitoring, quick diagnosis, and low cost. By combining the advantages of metal oxide semiconductor (MOS) gas sensors (fast-responding, affordable, and highly sensitive), the preponderance of MOS E-nose is further enhanced. This article focuses on metal oxide semiconductor gas sensors for detecting volatile organic compounds. The sensing principle and modification methods of binary and ternary metal oxide sensing materials are reviewed. It also encompasses a review of the metal oxide semiconductor electronic nose for detecting cancer and respiratory diseases.

1. Introduction

Early diagnosis of cancer can improve the chances of cure and survival time of patients appreciably. Among diverse approaches, breath analysis has been extensively studied due to its unique advantages, such as making it possible to quickly and painlessly diagnose diseases by testing the change of volatile organic compounds (VOCs) biomarkers contained in exhaled breath. VOCs are not only released from exhaled breath but also from various body fluids of the human body (Urine, Sweat) [1] while exhaled breath is the easiest to analyze [2]. Inert gases, water vapor, nitrogen, oxygen, and carbon dioxide make up the majority of human exhaled breath. Furthermore, exhaled breath also contains inorganic VOCs like nitric oxide, ammonia, and carbon monoxide along with organic VOCs such as ethane, acetone, and pentane. In 1971, Pauling et al. [3] first found that human exhaled breath contained over 200 VOCs. To date, about 3000 VOCs have been discovered in human breath [4]. Phillips et al. [5] used a combination of 22 VOCs as a "fingerprint" for lung cancer, discovering significant quantitative differences between the lung cancer and non-lung cancer groups. These VOCs had a sensitivity of 100% for differentiating patients with stage I lung cancer. By comparing the change of biomarkers in the exhaled breath which can reflect the metabolic status of human tissue cells, identifying plenty of diseases such as asthma, lung cancer, ovarian cancer, gastric cancer, and diabetes become reality.

Gas chromatography-mass spectrometry (GC-MS) technology is commonly utilized in breath analysis [6]. The sample is collected and pre-concentrated before being injected into the gas chromatography. The gas mixture will be separated and checked by gas chromatography and then ionized and analyzed by the mass spectrometry module. Combining the two methods provides a much higher accuracy and sensitivity, which makes it a suitable method for detecting the VOC trace for breath analysis. Monedeiro et al. [7] used headspace gas chromatography–mass spectrometry (HS-GC-MS) technology (a static headspace method) to detect VOCs from human sweat, differentiating cancer patients from controls successfully. Unlike GC-MS, proton transfer reaction mass spectrometry (PTR-MS) measures VOCs rapidly by chemical ionization reaction. In PTR-MS, H_3O^+ ions generated by the ion source trigger a proton transfer reaction with VOCs in the drift tube, and the resulting products are analyzed using the mass spectrometer [8]. This method can detect most of the VOCs and exclude interference from other gases in the air. Selective ion flow tube mass spectrometry (SIFT-MS), like PTR-MS, can detect compound isomers by employing various precursor ions

* Corresponding author. College of Mechanical Engineering, Yangzhou University, Huayang West Road 196, Yangzhou, 225127, Jiangsu Province, PR China.
E-mail address: zhangc@yzu.edu.cn (C. Zhang).

https://doi.org/10.1016/j.pnsc.2024.01.018
Received 19 December 2023; Received in revised form 23 January 2024; Accepted 28 January 2024
Available online 16 February 2024

(H_3O^+, O_2^+, and NO^+) [9]. In comparison to PTR-MS, the benefit of this method is that the sample is directly analyzed using a "breath head". Meanwhile, these techniques have some limitations, including the need for skilled professionals, the use of pricey instruments, the use of cumbersome analytical equipment, and high measurement costs.

As a result, it is urgent to develop an instrument with real-time analysis, user-friendly, portable, and non-invasive for early disease diagnosis. The electronic nose (E-nose) resembles the human olfactory system, including an array of gas sensors that react with the sample to produce a smell print, which is used by pattern recognition algorithms for classification. In 1961, Moncrieff [10] built the first machine olfactory instrument. In 1964, Wilkens and Hatman reported an early E-nose [11]. This instrument worked through redox reactions of the gas on the electrode. In 1965, Buck and Dravnieks et al. built E-noses by altering the conductivity and adjusting the contact potential. Persaud and Dodd [12] created a device for odor detection in 1982 by combining animal olfaction with semiconductor sensors. The device responds to odors, but it cannot recognize them since it doesn't have an odor memory. The solution is to expose it to multiple odors and locate the response in the memory. At a conference in 1987, the word "electronic nose" was used for the first time as a term [13]. For the past three decades, E-nose has now frequently utilized in food testing, environmental industries [14], agriculture, and medical diagnosis [15] due to its simplicity, speed, and accuracy in detecting gas mixtures. E-noses can recognize specific exhaled breath fingerprints with high accuracy, which makes them an ideal candidate for medical diagnosis. Metal oxide semiconductor (MOS) is a kind of metal oxide having semiconductor characteristics, which has a wide bandgap. MOS gas sensors are cheap, small, sensitive, and easy to fabricate, rendering them extensively employed in E-noses [16,17].

Unlike other reviews on detecting diseases in Table 1. This article focuses on MOS E-noses for detecting volatile organic compounds. The sensing principle and modification methods of binary and ternary metal oxide sensing materials including morphology modification, doping, and building heterojunctions are reviewed. This article also reviews the latest applications of MOS E-noses for detecting cancer and respiratory diseases and offers insights into potential avenues for enhancement and improvement of MOS E-noses.

2. E-nose

2.1. Breath makers

VOCs include endogenous VOCs and exogenous VOCs. Changes in endogenous VOCs can reflect metabolic and pathological processes in the human body [22]. Exogenous VOCs are absorbed into the body thus affecting the concentration of breath markers. Identifying appropriate breath biomarkers is a fundamental requirement for effective breath analysis. The selection of disease biomarkers necessitates a clear biological origin as well as sufficient clinical data to back it up [23]. The imbalance between reactive oxygen species (ROS) production and removal causes oxidative stress with many disease biomarkers produced [24,25]. For example, polyunsaturated fatty acid peroxidation produces alkanes, which have been linked to inflammatory and cancer-related diseases [26]. Patients with asthma, chronic obstructive pulmonary disease, and other lung diseases have more pentane and ethane in their exhaled breath [27,28]. One of the most prevalent breath VOCs is acetone. When the body does not produce enough insulin or cells are insulin resistant, fat is used to produce energy. The body then produces Ketogenesis, which further produces acetone. Its concentrations rise with an increased fatty acid oxidation rate, which is linked to weight loss and is used to monitor epilepsy and diabetes [29–31]. Table 2 shows some typical breath biomarkers used to detect different diseases.

Table 1
E-noses for detecting disease.

E-nose model	Target diseases	Year	Reference
Multivariate	Respiratory diseases	2017	[18]
Multivariate	Gastrointestinal Disease	2018	[19]
Multivariate	Diabetes	2020	[20]
Multivariate	Chronic obstructive pulmonary disease	2020	[21]
MOS-based	Cancer Respiratory diseases	2024	This work

2.2. Structure and working principle

E-noses can identify and distinguish a wide range of airborne substances (including headspace volatiles from any source). An array of gas sensors, a signal processing system, and a pattern recognition algorithm make up a standard E-nose. It is similar to the human olfactory system (Fig. 1). Receptor neurons receive stimuli from the environment, such as odorous substances, and generate corresponding signals. These signals are then transmitted to the brain for further processing and interpretation. Finally, neurons are able to distinguish between odors. The airbag collection method, storing the subject's end-tidal breath samples in a Tedlar bag [41], is the typical offline breath analysis method used for the study. Utilizing online breath analysis is a better strategy because it prevents contamination of the exhaled breath sample and allows for real-time analysis. After bringing the sample into the E-nose through the above methods, the gas undergoes a chemical reaction with the sensitive material present in the sensor array, resulting in the conversion of the chemical signal (such as gas type and concentration) into an electrical signal. After signal processing (preprocessing, filter, exchange, and feature extraction), the electrical signal is transformed into a digital signal. The extracted feature vectors are inputted into suitable pattern

Table 2
Exhaled breath markers of disease.

Disease	Biomarker	Technology	Reference
Lung Cancer	Benzaldehyde 2-ethyl hexanol 2,4-decade-1-ol	GC-Q-TOF/MS	[32]
Prostate cancer	Hexanal 2,5-Dimethylbenzaldehyde Hexan-2-one 2,6-Dimethyl-6-hepten-2-ol	HS-SPME-GC-MS	[33]
Breast Cancer	Cyclotetrasiloxane Tetradecane 2,7,10-trimethyl dodecane 2-hexyl-1-octanol	GC-MS	[34]
Gastric cancer	3-octanone Butanone	HS-SPME-GC-MS	[35]
Chronic obstructive Pulmonary disease	Acetone 1,2-pentadiene toluene butyrolactone	GC-MS	[36]
Tuberculosis	1-methyl-1- 1,4-dimethyl-cyclohexane , C4–C20 alkanes monomethylated alkanes	GC-MS	[37]
Novel coronavirus	Acetaldehyde Octanal Acetone Butanone Methanol	GC-IMS	[38] [39]
Diabetes	Ethanol Isopropanol Dimethylsulfid Isoprene Pentanal	PTR-TOF-MS	[40]

Notes: GC-MS: Gas chromatography-mobility spectrometry, GC-IMS: Gas chromatography-ion mobility spectrometry, HS-SPME-GC-MS: Headspace solid-phase microextraction coupled with gas chromatography-mass spectrometry, GC-Q-TOF/MS: Gas chromatography quadrupole time of flight/mass spectrometry, PTR-TOF-MS: Proton-transfer-reaction time-of-flight mass spectrometers.

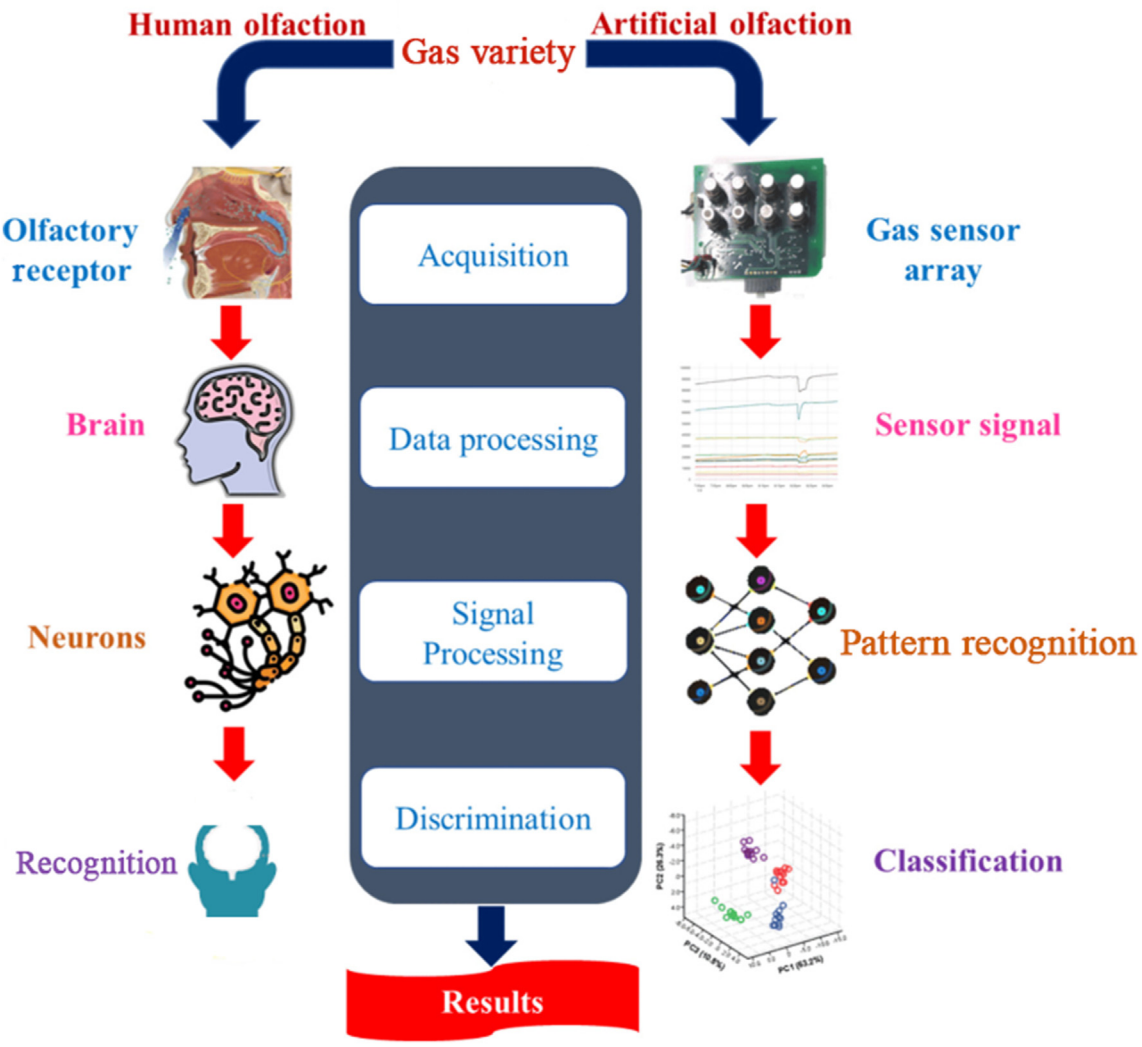

Fig. 1. Typical signal collection, processing, and discrimination of an electronic nose system.

recognition algorithms, which construct models by learning from sample data with known odor patterns. These models are then used to classify and recognize unknown samples based on their learned odor patterns [42].

Table 3
Summarizes the advantages and disadvantages of gas sensors used in E-nose.

Sensor	Advantage	Disadvantage
MOS	Low price, high detection sensitivity, and fast response speed	Don't have a good selection, high-energy consumption, and high working temperature
CP	High sensitivity and fast response time, capable of detecting many different types of gases	Vulnerable to environmental influences, special calibration required
MPSE	Works in a wide range of temperatures and moisture conditions, highly precise	Sensitive to vibration, shock, and mechanical Damage
CM	Excellent sensitivity; quick response time and precise detection	Demanding purity and handling of samples, costly and subject to moderation
QCM	Highly sensitive; rapid response; high accuracy and stability	More costly; may be susceptible to environmental vibrations and disturbances

Notes: MOS: Metal Oxide Semiconductor, CP: Conducting polymers, MPSE: Mixed-potential type solid-state electrolyte, CM: Colorimetric, QCM: Quartz Crystal Microbalance.

2.2.1. *Gas sensors*

Different materials and types of sensors are used in E-noses. Table 3 lists the benefits and drawbacks of several commonly used sensors.

One of the most popular types of sensors is the MOS gas sensor. Raspagliesi et al. [43] diagnosed ovarian cancer (OC) using an E-nose comprised of ten MOS gas sensors over 251 subjects: 114 healthy people, 86 OC patients, and 51 benign patients. Different MOS sensors are sensitive to various VOCs, improving the diagnostic capability of the E-nose. The resistance signal of the baseline (R0-ohm) is subtracted from the resistance signal of the sensor (R-ohm) and divided by the resistance signal of the baseline (R0) to obtain the response of the sensor. Three sensors displayed a significant increase in signal in the OC case. The sensitivity and specificity of the K-Nearest Neighbor (K-NN) classification model to distinguish between OC patients and controls were 98% and 95% respectively, and 89% and 86% for the distinguishing of OC patients, benign patients + controls.

Due to their high selectivity at room temperature, conducting polymer (CP) sensors are widely used in the electronic nose field. The Cyranose-320 (C-320) electronic nose is made of 32 sensors, each of which is covered in a variable carbon composite polymer film. Pier et al. [44] used the C-320 E-nose to detect VOCs in urine headspace and successfully distinguished bladder cancer patients and controls. However, the CP sensor is sensitive to humidity and has poor repeatability.

Quartz Crystal Microbalance (QCM) sensors have low detection limits and a quick response speed [45]. Zetola et al. [46] employed a QCM

E-nose to diagnose pulmonary tuberculosis with 94.1% and 90% differentiation sensitivity and specificity, respectively.

In comparison with other sensors, MOS gas sensors are more common in E-noses owing to their low cost, high reliability, rapid response, and ease of integration. MOS sensors are based on the principle that gas molecules are adsorbed on the surface of a semiconductor to produce a redox reaction that changes the resistance value. The oxidation behavior of target gases is intricately dependent on the structural configuration, morphological attributes, porosity characteristics, and operational temperature of the host matrix material [47]. In Fig. 2, when the p-type semiconductor NiO contacts air, oxygen molecules gain electrons from the conduction band of NiO, resulting in hole-accumulation layers (HAL) on the sensor surface. This will lower the resistance of the sensor. The hydrogen then reacts with oxygen ions, releasing electrons back to NiO, resulting in a decrease in HAL thickness and an increase in the resistance of the sensor.

VOCs are present in low concentrations at breath-realistic conditions. Changing the chemical composition, regulating the crystal structure, and using nanoparticles can significantly improve the sensitivity and selectivity of MOS gas sensors. Formaldehyde should be tested at 100pbb when mixed with other exhaled compounds (ammonia, acetone). A single MOS sensor hardly has sufficient sensitivity and selectivity. By doping the sensors and forming them into an array, the average error in measuring formaldehyde is only 9 ppb [48]. Specific sensitization measures for metal oxide sensing materials will be presented in Section 3.

2.2.2. Data analysis

It is challenging to improving the selectivity and specificity of individual gas sensors, assembling multiple sensors into cross-reactive sensor arrays and processing the signals with pattern recognition techniques can effectively address this issue. The electronic nose is capable of simultaneous detection of multiple gases, where each sensor exhibits unique responses to specific gases. Following the acquisition of these responses, feature extraction techniques are applied, and subsequent data dimensionality reduction is performed. Advanced data processing methods are employed to compute relevant information, thereby enhancing selectivity for specific gases. Pattern recognition (PR) is a decision vector that classifies objects according to a pattern and characterizes complex mixtures to identify individual components qualitatively and quantitatively. Principal Component Analysis (PCA), Linear Discriminant Analysis (LDA), Artificial Neural Network (ANN), K Nearest Neighbors (KNN), Support Vector Machines (SVM), and Random Forest (RF) are commonly utilized [50]. PCA is an unsupervised method that transforms a set of possibly correlated variables into a linearly uncorrelated set of variables by orthogonal transformation [51]. PCA serves as a valuable tool for data analysis and feature extraction. It can be effectively combined with other pattern recognition algorithms to enhance data separability and improve model performance. LDA is employed to reduce the dimensionality of data, thereby facilitating analysis and interpretation. By reducing the dimensions, LDA enables improved separation between different categories and enhances the accuracy of categorization. KNN is a supervised learning method that can be applied to both classification and regression tasks. It offers the advantage of fast model training. SVM relies on only a few critical sample points and is not affected by a large number of non-critical samples. This makes SVM robust to data noise and outliers and can effectively avoid overfitting problems. RF is capable of making predictions and classifications by integrating multiple decision trees and synthesizing their results to arrive at a final decision. Polat et al. [52] used PCA to reduce a dataset with 57 features to 4 features in the detection of lung cancer. However, PCA struggles with non-linear data [53]. The supervised method known as artificial neural networks (ANNs) is widely applied. Given that they are made up of extensive networks of nodes, they resemble biological neural networks [54]. ANNs can process different types of input data by simulating the neural system of the human brain. They also have intelligent adaptive learning capabilities, making them suitable for use in nonlinear problems. Van de Goor et al. [55] used an E-nose to diagnose recurrent head and neck cancer. The ANN model successfully distinguished healthy

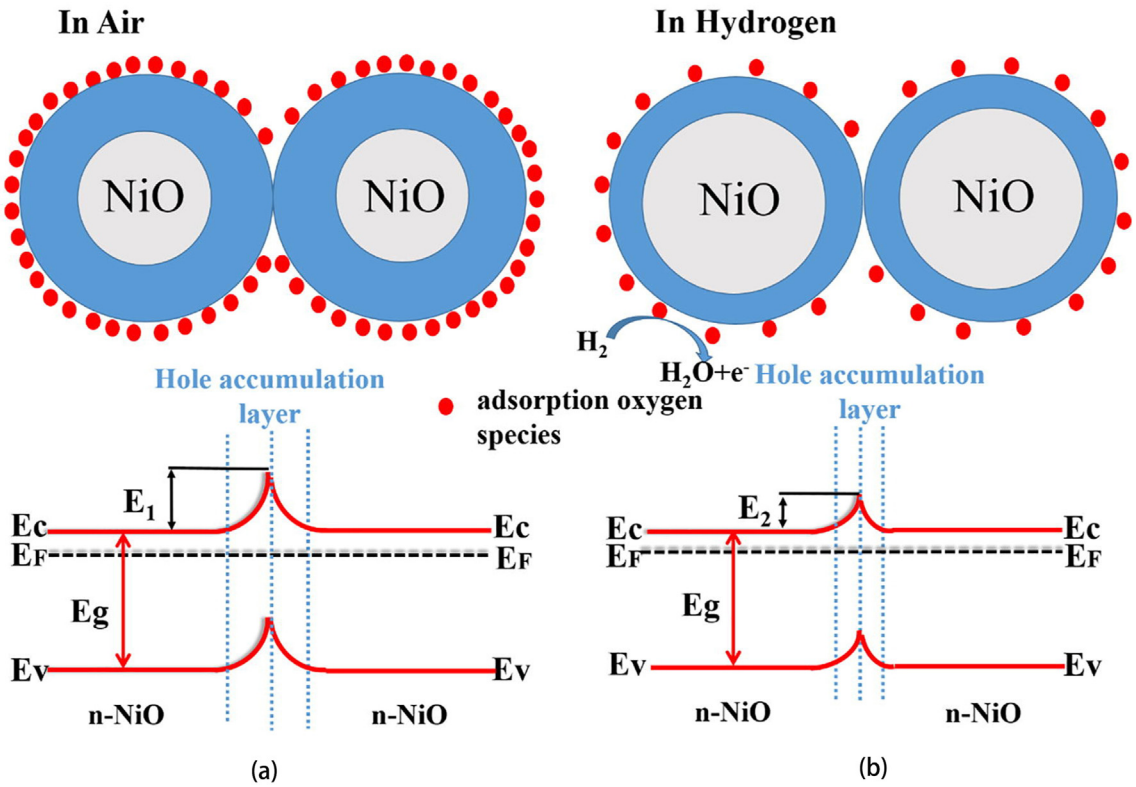

Fig. 2. Schematics of hydrogen gas sensing mechanism for NiO sensor [49].

and diseased populations with 85% sensitivity. Table 4 shows some of the algorithms used in E-noses. It can be seen that in E-noses detection, a combination of algorithms is frequently used to achieve the best classification results.

3. Metal oxide sensing materials

The MOS gas sensor is the fundamental part of E-nose, therefore enhancing the sensor's functionality is the key to raising E-nose's diagnostic precision. In this section, metal oxide sensing materials are classified into binary metal oxides and ternary metal oxides, which are described according to the construction of unique morphologies, doping of noble metals, and construction of heterojunctions.

3.1. Binary metal oxide

3.1.1. SnO_2

SnO_2 is an n-type metal oxide semiconductor with a 3.6 eV band gap. Due to its excellent reactivity to VOCs in exhaled breath, SnO_2 is a viable gas sensor material for the E-nose.

Nanostructures have a large specific surface area, allowing for significant improvements in the performance of sensing materials. Kuang et al. [61] synthesized 3D hierarchical SnO_2 nanostructures by hydrothermal method. Experimentally, the reaction rate was accelerated with the addition of higher NaOH concentration, leading to a faster nucleation rate and a smaller size of SnO_2. Thus, sample S3 has the finest nanorods and the highest density. Sample S3 exhibited twice the response of samples S1 and S2 when tested for ethanol, responding to 50 ppm ethanol for only 4 s at 150 mA with a recovery time of less than 2 s. The reason for the good response of S3 is that its nanorods have a diameter of 15–20 nm, similar to the Debye screening length. The highest nanorod density is seen in S3, thus boosting specific surface area and making it easier for oxygen species to interchange. The fine grain size and 3D hierarchical nanostructure can also be used to explain the good sensing properties of this SnO_2 material. Choi et al. [62] synthesized a bridge nanosheet structure of SnO_2 with a better response than conventional nanosheets. This bridge structure introduces space under the membrane, providing an additional site and sufficient time for the reaction. The SnO_2 sensor thus fabricated showed excellent response to nonanal (Lung Cancer marker) and has the potential to be used in E-nose to detect lung cancer. This shows that creating nanostructures is a successful strategy for improving sensor performance.

Doping can create oxygen vacancies and dislocations, providing more active sites. Saasa et al. [63] synthesized a SnO_2 sensor doped with 9 at% Co by hydrothermal method, showing a maximum sensitivity of 45.8 for 5 ppm acetone (an exhaled breath marker for diabetes). Additionally, this sensor has good selectivity and a low detection limit for acetone (0.5 ppm). Cobalt doping increased the surface area of SnO_2 by 210%, reduced the pore size by 22%, and increased the response to acetone by 112%. The temperature ranged from 50, 100, 150, 200, and 250 °C for the experiments. The best operating temperature including WO_3–Co and VO_2–Co sensors was 100 °C, indicating that the Co doping reduced the operating temperature of the sensors. Moreover, all of these sensors responded highly to acetone at 100 °C. This demonstrates that adding Co is a useful technique for increasing the n-type sensing materials' acetone sensitivity. However, human exhalation is rich in water vapor. This experiment showed that the response of the sensor to acetone was reduced by more than half under conditions of humidity. The reason behind this is that water vapor occupies the adsorption sites of the gas to be measured and the adsorbed oxygen on the sensitive material is reduced, resulting in a decrease in sensor performance. Van Duy et al. [64] decorated SnO_2 with Ag (1 nm) and Pt (2 nm) and the sensor showed a good response (4.31) and response time (12 s) to 1 ppm NH_3 at 250 °C operation. This sensor was tested repeatedly at several humidity levels (0–90% RH) and the outcomes revealed no appreciable decrease in sensor response, probably due to the high temperature promoting the desorption of water vapor. Reducing the effect of humidity on measurements when testing exhaled gases with an E-nose is still a problem.

The composite material enhances the performance of the sensor and reduces sensitivity to moisture. Narjinary et al. [65] compounded Multi-walled carbon nanotube (MWCNT) into SnO_2, and the sensor showed the highest response at 0.25 wt% of MWCNT (Fig. 3 (b)). The sensor's performance had significantly enhanced (Fig. 3). MWCNT's large surface area and excellent adsorption capacity enhanced the adsorption capacity of SnO_2. Moreover, the difference in the work function of MWCNT and SnO_2 facilitates the transfer of electrons. However, adding too much MWCNT makes the number of electrons at the grain boundaries increase, which reduces the performance of the sensor (Fig. 3 (b)). By constructing a heterojunction, this sensor is capable of measuring 1 ppm acetone effectively and is not sensitive to moisture. Graphene-based binary nanocomposites form tight electrical contacts through heterostructure, enabling electrical and electronic modifications to occur simultaneously. Marappan et al. [66] prepared graphene oxide (GO)/SnO_2 binary nanocomposites with good response to acetone at room temperature and visible light. In conclusion, SnO_2-based gas sensors can improve sensitivity through building nanostructures, doping, loading, and constructing heterostructures. The content needs to be controlled to obtain the optimal ratio when doping or compounding. Lowering the optimal sensor operating temperature while reducing the effect of moisture on the sensor remains a challenge for exhaled breath detection using E-noses.

3.1.2. ZnO

ZnO is a typical n-type semiconductor with a wide band gap (3.37 eV) and has already been widely used in MOS sensors [67].

Bian et al. [68] fabricated ZnO nanosensors with high performance to acetone by electrospinning technique combined with calcination. ZnO nanoparticles underwent two and 12 h of calcination, respectively. The longer calcined ZnO had a multi-vacancy network structure and more oxygen vacancies with a higher response than the former at 340 °C. In addition, the sensor showed good stability with a nearly constant sensor signal for 120 days. Zhang [69] et al. fabricated a ZnO sensor using the peroxide thermal decomposition method, which is rich in oxygen vacancies. The sensor exhibits excellent response to 1 ppm NO_2 at room temperature under visible light illumination.

Systematic impurity doping can serve as a viable approach to reduce size and enhance the electrical conductivity of materials, thereby resulting in notable improvements in the performance of gas sensors [70]. Yoo et al. [71] doped 1 at% Al, Co, and Cu into ZnO nanoparticles (NP) via the hydrothermal method, and the Al-doped sensor responded the most to acetone at 500 °C (11.8). It can be seen in Fig. 4 that Al performed better as a dopant than Cu and Co because the Al-doped ZnO nanoparticles possess dioxygen vacancies that create deep donor-level defects [72]. Through the application of chemical spray pyrolysis, Kathwate et al. [73] prepared Al-doped ZnO films. It was found that the lattice parameters of the ZnO films gradually decreased with Al doping,

Table 4
Data analysis method Applied in medical diagnosis electronic nose.

Diseases	Sensor	Data analysis method	References
Diabetes Mellitus and Chronic Kidney Disease	MOS	PCA、SVM、HCA、PLS	[56]
Chronic obstructive pulmonary disease and Lung cancer	MOS	KPCA、XGBoost、AdaBoost、RF	[57]
Chronic liver disease	QCM	PLS-DA	[58]
Colorectal cancer	CP	PCA、CDA	[59]
Lung cancer	CP	LRA	[60]

Notes: PCA: Principal Component Analysis, SVM: Support Vector Machines, LRA: Logistic regression analysis, PLS: Partial Least Squares, KPCA: Kernel Principal Component Analysis, CDA: Canonical Discriminant Analysis, XGBoost: Extreme Gradient Boosting, AdaBoost: Adaptive Boostin, RF: Random Forest, HCA: Hierarchical Cluster Analysis, PLS-DA: Partial Least Square Discriminant Analysis.

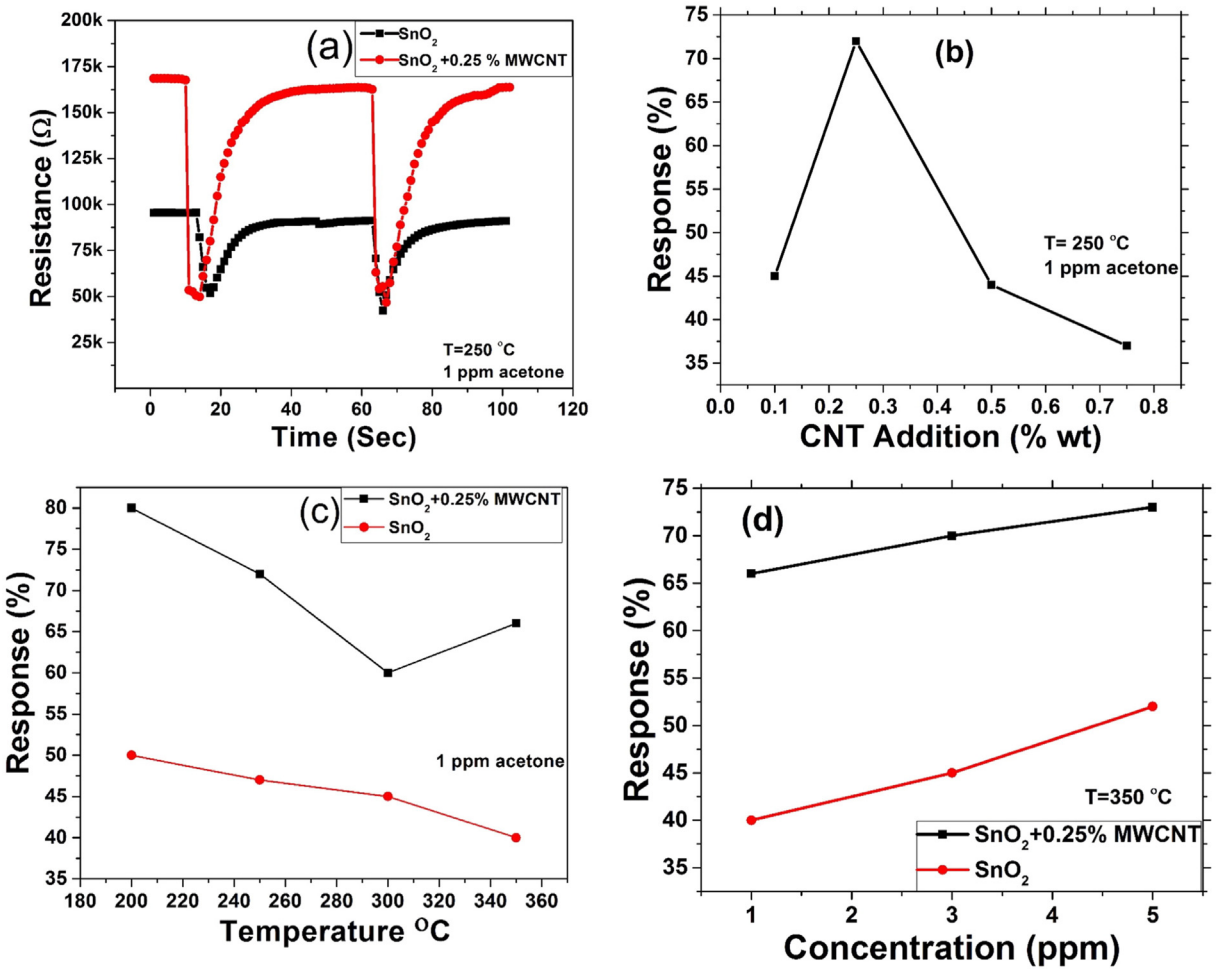

Fig. 3. (a) Response of SnO_2 and SnO_2-0.25% MWCNT sensors in 1 ppm acetone at 250°C. (b) Response of SnO_2 sensor in 1 ppm acetone for different CNT loadings at 250°C. (c) Response of SnO_2 and SnO_2-0.25% MWCNT nanocomposite sensors in 1 ppm acetone at different temperatures. (d) Response of SnO_2 and SnO_2-0.25% MWCNT sensors in different concentrations of acetone at 350°C [65].

which indicated that Al was indeed doped into the lattice of ZnO. Al caused significant changes in both strain and stress in the ZnO lattice. The ZnO transformed from hexagonal to spherical particles and reached the minimum average grain size (19.84 mm) when the Al content reached 3%. The sensor responds well to low concentrations of NH_3 (25 ppm) at 100 °C. It is also superior to pure ZnO in terms of response and recovery time. Sankar Ganesh et al. [74] doped ZnO with 6 wt% Al and also obtained a sensor with a high response to NH_3. This indicates that Al doping does have a general improvement for ZnO sensors. Detection of NH_3 in human breath enables the diagnosis of kidney disease and asthma, and the use of Al-doped ZnO is a favorable option.

Similar to SnO_2, heterojunctions can significantly enhance ZnO sensing performance. Zhang et al. [75] used the room-temperature liquid phase method to composite 1–2 μm ZnO with GO. This three-dimensional structure has heterojunctions with abundant cavities and a large surface area, providing the gas with more pathways and reactive sites for diffusion and adsorption, as well as lowering the operating temperature. It can be seen in Fig. 5 that the GO/ZnO sensor has 5.9 times the response value of ZnO at 180 °C, and the density functional theory confirms its excellent selectivity for acetone. GO and ZnO form a p-n heterojunction with different Fermi energy levels, leading to the transfer of holes and electrons. This creates a space charge layer on the heterojunction. This causes the energy band to bend at the junction to create a potential barrier, hindering electron transport. Thus the initial resistance of the sensor becomes higher and the response becomes more pronounced. Reduced graphene oxide (rGO) is also a commonly used composite material. Gupta et al. [76] prepared rGO-ZnO nanocomposites using 1 mg/mL of GO precursor dispersion by in situ hydrothermal method. At room temperature operating temperature, the rGO-ZnO sensor was not sensitive to humidity and responded to NH_3 significantly stronger than other gases. The extremely small nanoparticle size provides more charge compensation sites for the nanocomposites, and rGO has excellent electrical conductivity. This can be used to explain why pure ZnO cannot respond to NH_3 at room temperature, while rGO-ZnO can. However, when the rGO exceeded the optimum value, the synergistic effect between the two materials tended to favor p-type rGO, which led to a decrease in performance. Zhang et al. [77] doped Au into nano-ZnO to construct nanocomposites with a porous structure, which greatly enhanced the response to benzene. The team then synthesized Au–ZnO and Exfoliated WSe_2 using a self-assembly technique to make a sensor that was highly responsive to benzene, highly selective and reproducible, and capable of operating at room temperature. This was attributed to the doping of Au and the formation of heterojunctions. The issues of MOS sensors, such as their high working temperatures, poor selectivity, and susceptibility to humidity, are being resolved by obtaining smaller nanometer sizes, doping other metals, and building heterogeneous structures. Finding the best doping or composite substance and finding the optimal content is the direction of future work.

3.1.3. TiO_2

As an n-type semiconductor, TiO_2 is commonly manufactured by hydrothermal, electrospinning, and anodization methods to obtain

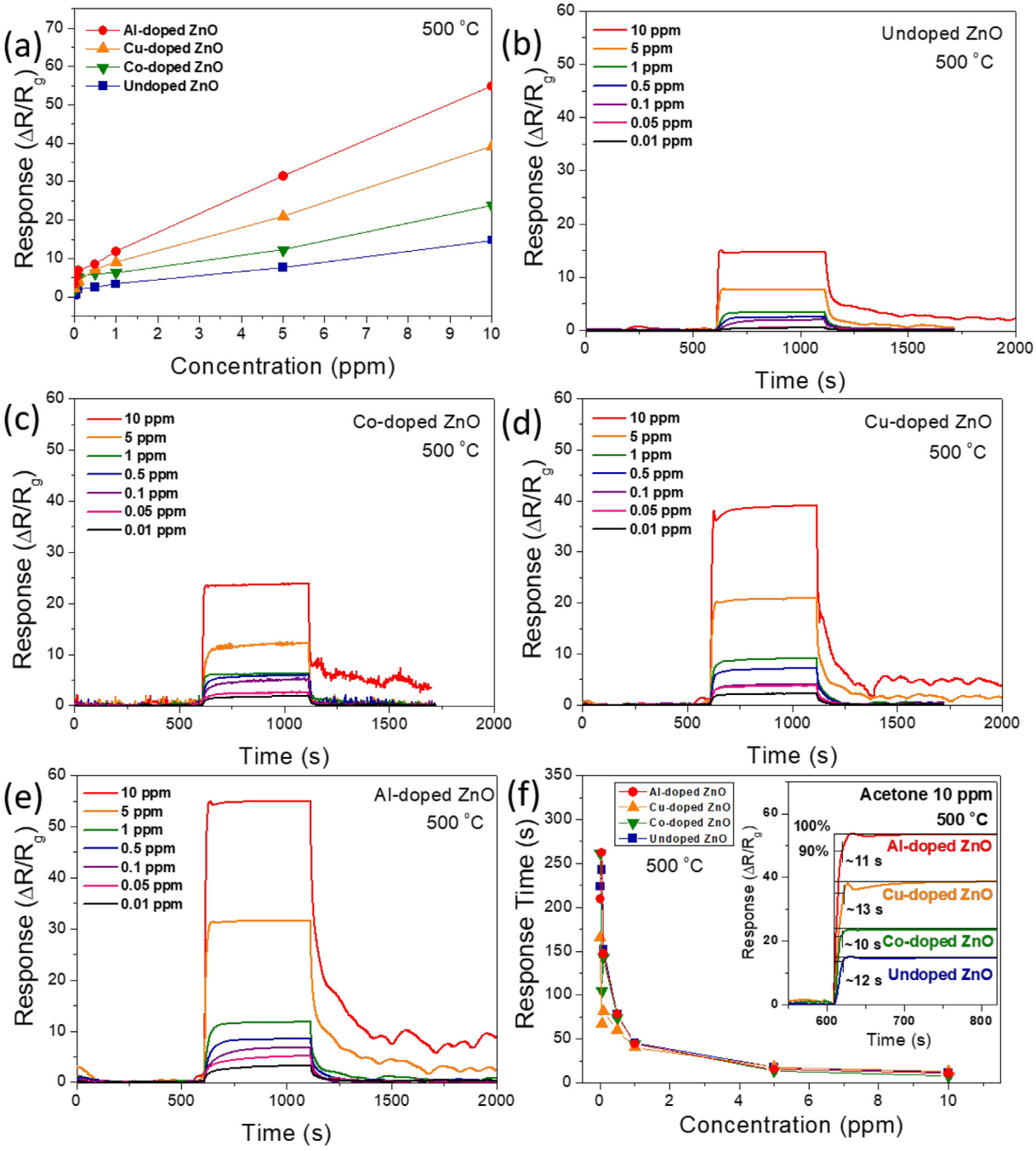

Fig. 4. (a) Sensing responses of the undoped and Co-, Cu-, and Al-doped ZnO NPs to different concentrations of acetone in the range of 0.01-10 ppm at the optimal operating temperature of 500°C. (b)-(e) Variations in the responses of the undoped and Co-, Cu- and Al-doped ZnO NPs during the detection of acetone at different acetone concentrations in the range of 0.01-10 ppm at 500°C. (f) Response time as a function of the acetone concentration (0.01-10 ppm) at 500°C. The inset shows the estimation of the response time of all the samples upon exposure to 10 ppm acetone [71].

structures in the form of tubes, rods, and fibers, resulting in sensors with high sensitivity [78].

A key to assembling E-nose with MOS gas sensors is the miniaturization and integration of the sensors, which requires sensing materials with high position controllability and uniformity. Kimura et al. [79] fabricated TiO_2 nanotube sensors on Si substrates using photolithography and anodization. This sensor was 3 μm long and 100 μm wide, respectively, and had a high sensitivity to H_2. This shows that anodization is an effective method to miniaturize the sensor. To use this sensor effectively for electronic nose diagnosis, the team used Pt to modify TiO_2 nanofilms by atomic layer deposition technique [80]. The response of the sensor modified with Pt was improved by 7 orders of magnitude compared to the original sensor for H_2, and it also showed good response for CO. They integrated multiple TiO_2 sensors and combined mechanical learning and neural networks to achieve predictions within 0.001% accuracy for 0.02% CO concentration [81]. This accuracy is sufficient to detect CO in exhaled breath in cases of abnormal lung function. The nano-structuring of TiO_2, the sensitization with Pt, the reduction of sensor size using anodic oxidation, and finally integrating multiple sensors and combining them with machine algorithms to achieve accurate detection of specific gases in gas mixtures is an effective research direction.

3.1.4. Others

NiO, In_2O_3, WO_3, Al_2O_3, CuO, Fe_2O_3, and MoO_2 have also been used

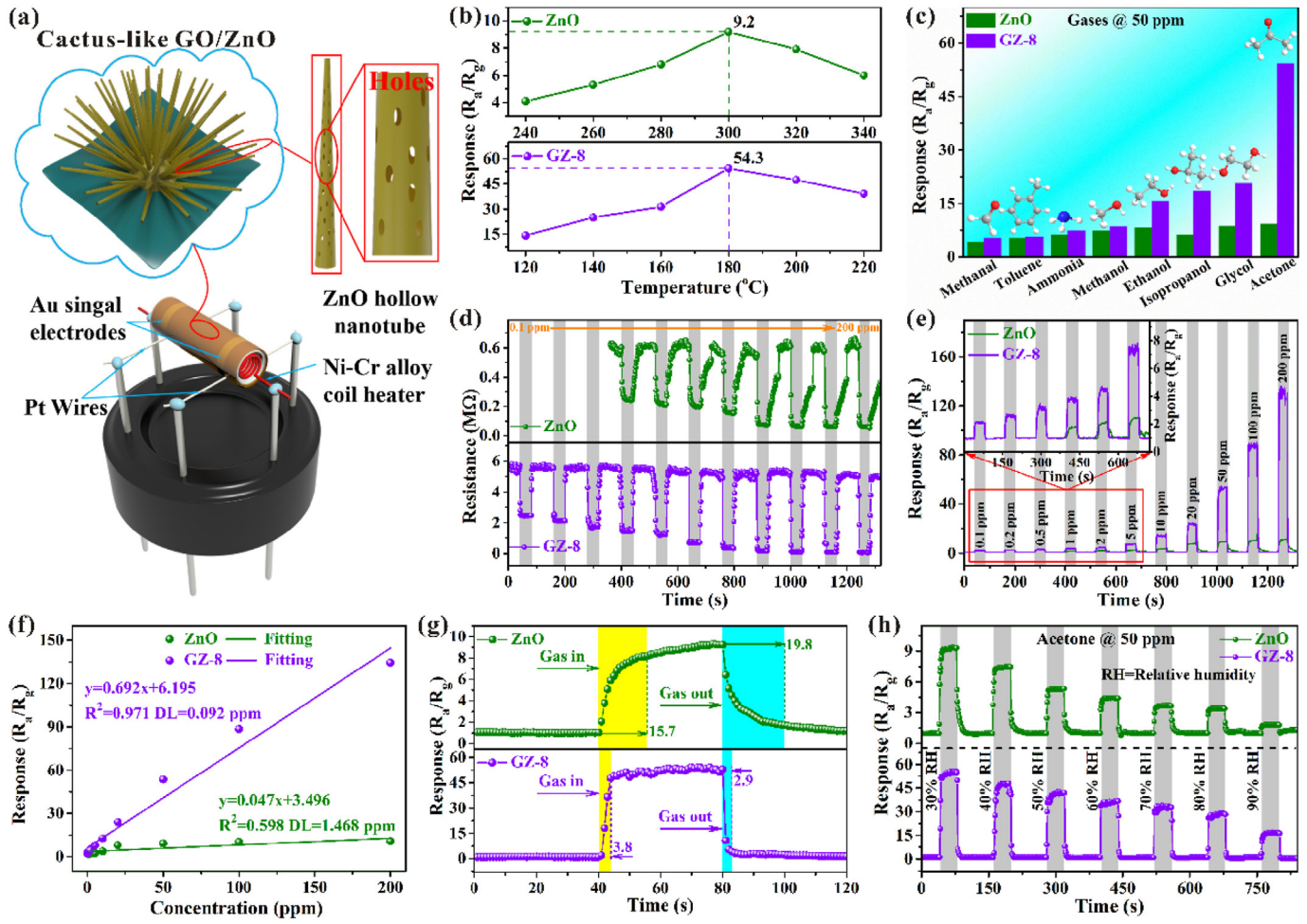

Fig. 5. (a) GO/ZnO gas sensor. (b) Response of pure ZnO and cactus-like GZ-8 based sensors to acetone (50 ppm) at different operating temperatures. (c) Response of pure ZnO and cactus-like GZ-8 based sensors to 50 ppm different VOCs at 180°C. (d, e) Resistances cycles, response-recovery cycles, and fitted curves corresponding to the response values of pure ZnO and cactus-like GZ-8 based sensors towards 0.1-200 ppm of acetone at 180°C. (g) Response/recovery curves of pure ZnO and cactus-like GZ-8 based sensors in the presence of acetone (50 ppm) at 180°C. (h) Cyclic response/recovery curves of pure ZnO and cactus-like GZ-8 sensor to 50 ppm acetone under different relative humidity [75].

Table 5
Binary sensitive material for the detection of exhaled breath markers.

Materials	Synthesis route	Target gas	Gas Concentration	Operating temp (°C)	Response	Response and Recovery Time (s)	Reference
NiO	Sol-gel	NH_3	0.4 ppm	RT	91.2[a]	54/58	[82]
PdO/NiO	Electrochemical deposition	H_2S	10 ppm	155	515.27[a]	50/7	[83]
NiO/ZnO	Hydrothermal	ethanol	100 ppm	350	54[b]	–	[84]
ZnO–SnS_2	Hydrothermal	H_2S	30 ppm	180	0.712[e]	10/51	[85]
Ag–In_2O_3	Soft template	isopropanol	1ppm	300	2.2[d]	12/175	[86]
ZnO–In_2O_3	Soft template	NO_2	100 ppb	75	805.2[a]	800/200	[87]
Pt–In_2O_3	Hydrothermal	isoprene	5ppm	200	103.5[b]	124/204	[88]
Au-sputtered WO_3	Thermal oxidation	H_2S	5ppm	350	163[d]	240/1200	[89]
WO_3–TiO_2	Spin coating	H_2	1000 ppm	RT	0.7821[c]	20/23	[90]
MXene/Co_3O_4	Hydrothermal	formaldehyde	10 ppm	RT	9.2[a]	83/5	[91]
Ga_2O_3/Al_2O_3	Hydrothermal and calcining	NO_x	100 ppm	RT	0.582[e]	–	[92]
CuO	Wet chemical	acetaldehyde	100 ppm	180	4.18[c]	–	[93]
MoS_2–CuO	Precipitation	acetone	10 ppm	RT	16.21[a]	61/85	[94]
CuO/rGO	Hydrothermal	ethanol	100 ppm	175	10.54[a]	32/446	[95]
CuO/rGO	Hydrothermal	NO_2	5ppm	RT	4.008[d]	6.8/55.1	[96]
PdO–CuO	Impregnation	H_2S	50 ppm	30	6.8[b]	1.8/4.1	[97]
α-Fe_2O_3	Uniform-micro spherical carbon templates	acetone	25 ppm	350	98[b]	2/-	[98]
Pt-α-Fe_2O_3	Solvothermal	acetone	100 ppm	175	105[b]	2/355	[99]

Notes: a. R_g/R_a, b. R_a/R_g, c. $(R_g-R_a)/R_a$, d. $(R_a-R_g)/R_g$. e $(R_a-R_g)/R_a$.

to detect gases in exhaled breath. Table 5 shows some of their existing studies.

As shown in Table 5, the construction of nanoporous structures, the doping of precious metals, and the use of composite materials to build heterogeneous structures can effectively reduce the operating temperature of MOS sensors.

Sensors operating at high temperatures will respond and recover quickly since the gas is involved in the reaction at a faster rate. However, low-temperature sensors do not have high temperatures to assist the reaction to proceed, resulting in longer response and recovery times. Zhang et al. [100] fabricated an In_2O_3 nanowire sensor by the electrospinning method. It could precisely detect 10 ppb of NO_2 at 25 °C. As the temperature continues to increase, the equilibrium between adsorption and desorption of the gas arrives earlier, which can lead to a lack of depth in the reaction, reducing the response of the sensor. But this sensor had a recovery time of up to 1000 s. The team then irradiated the sensor with different intensities of visible light and showed that the stronger the visible light, the shorter the recovery time of the sensor. However, excessively strong light would make the sensor resistance change rapidly after being removed from the light, and cannot maintain a stable state. Finally, 4.58 mW/cm^2 was determined to be the optimal visible light intensity to reduce the sensor recovery time to 20 s. Visible light irradiation is an easy method to reduce the recovery time. Zhang et al. [101] doped Co in In_2O_3/MoS_2 composite for room temperature detection of CO. Co–In_2O_3/MoS_2 has a nanorod-like structure (Fig. 6), increasing the surface area. Moreover, the doping of Co generates more oxygen vacancies in the material and forms impurity energy levels, which facilitates the transport of electrons and thus enhances the performance of the sensor. The n-n type heterojunction formed among Co–In_2O_3 and MoS_2 also contributes to the reaction.

Lei et al. [99] doped 2 at% Pt into α-Fe_2O_3, resulting in a 2.5-fold improvement in sensor performance. Given that with the addition of Pt, the sensitive material has a smaller band gap more conducive to electron transport and generates a large number of oxygen vacancies. This sensor had a very low detection limit, capable of accurately detecting 20 ppb acetone, and still maintained good sensitivity at 90% RH humidity, making it well suited for diabetes screening.

MoO_2 has high electronic conductivity and thermal stability and has

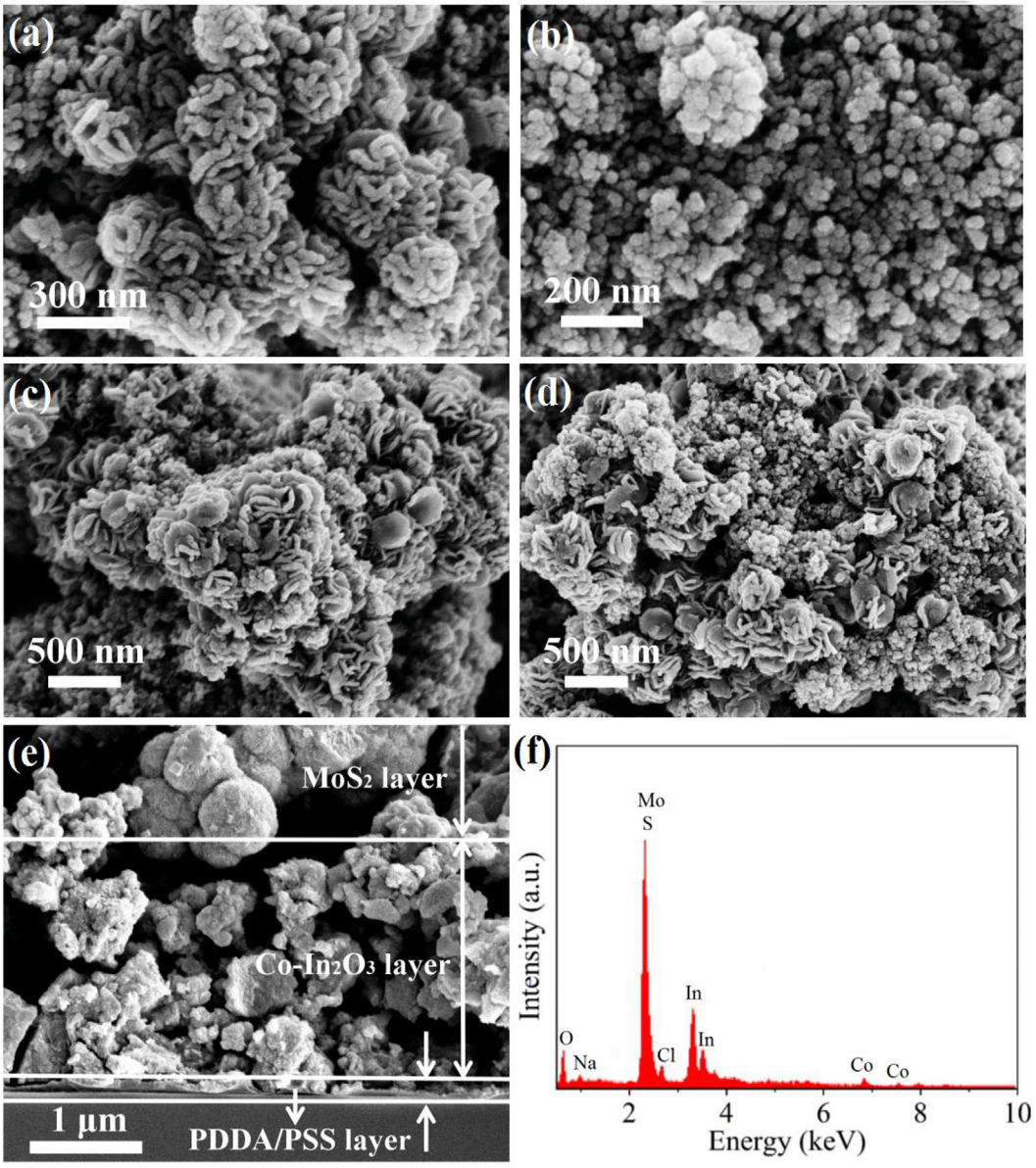

Fig. 6. SEM characterizations of (a) MoS_2, (b) Co-In_2O_3, (c) and (d) Co-In_2O_3/MoS_2. (e) Cross-sectional image of Co-In_2O_3/MoS_2 film on the substrate, (f) cross-sectional EDS spectrum of Co-In_2O_3/MoS_2 film [101].

been used to detect ethanol. Mehmood et al. [102] synthesized a MoO_2–Ni-GO composite. After being annealed at 400 °C, this material responded with 105–1000 ppm ethanol at room temperature and showed excellent selectivity. This was because of the increase in surface-adsorbed oxygen and hydroxyl groups in the composite with increasing annealing temperature, which promoted electron conduction and resulted in more electrons being trapped in the composite and reduced the sensor resistance. Moreover, the inherent resistance to the humidity of NiO made this sensor operate sensitively even at 90% RH humidity conditions. In addition, the sensor's selectivity is significantly influenced by the lowest unoccupied molecule orbit (LUMO). The LUMO value of ethanol is only 0.13 eV, which is much lower than formaldehyde (0.22 eV), methanol (0.2 eV), and acetone (0.21 eV), and this facilitates the electron transport between the composite and ethanol, resulting in a better selectivity of the sensor for ethanol.

3.2. Ternary metal oxide

Ternary metal oxide materials, consisting of two metal elements and oxygen, have emerged as a recent research hotspot in the field of gas sensors. This section focuses on the improvement of the sensing performance of ternary metal oxides by topography control and Chemical composition modification.

Hanh et al. [103] prepared three types of Zn_2SnO_4 in hollow octahedra, hollow cubes, and nanoparticles to compare their sensing properties. The octahedral Zn_2SnO_4 has a hollow structure consisting of 20 nm thick nanoplates. The voids between adjacent nanoplates provide a porous structure for the octahedral and increase the gas adsorption sites. Although nanoparticles have the largest specific surface area (64.066 m^2/g), their smallest pore size value (5.0 nm) limits the penetration of gas molecules inside them. The octahedron has the largest pore size (13.76 nm), providing sufficient diffusion space for gas molecules, so it showed a higher response to acetone than nanoparticles. The octahedral structure exhibited the highest response values in sensing tests for acetone, methanol, NH_3, H_2, and CO, with a response of 63.93 for 125 ppm acetone at 450 °C and a theoretical detection limit of 0.67 ppb, which is sufficient for the detection of diabetes. The response of the cubic structure was higher than that of the octahedral structure in the detection of ethanol, and the reason for this occurrence has not been determined. In addition to porous structures, heterogeneous structures can also enhance sensing performance. Wu et al. [104] synthesized $CuFe_2O_4$ hollow microspheres using a solvothermal method and annealing treatment process. Compared to the response of 1.6 shown by $CuFe_2O_4$ nanoparticle-based sensors towards 20 ppm NH_3 [105], this $CuFe_2O_4$ sensor exhibits a notably enhanced response of 4.0 towards 10 ppm NH_3 at 100 °C. The enhanced response of the CuFe2O4 hollow microspheres can be attributed to their significantly enlarged specific surface area and layered structure, which facilitate an increased number of surface adsorption sites and reaction zones. Ma et al. [106] constructed an n-n heterojunction between Zn_2SnO_4 and SnO_2 via hydrothermal method and calcination and obtained Zn_2SnO_4/SnO_2 with a hollow cubic structure. There are differences in the work functions of Zn_2SnO_4 and SnO_2. Before reaching Fermi level equilibrium, electrons in Zn_2SnO_4 continuously migrate into SnO_2, allowing the oxygen molecule to gain more electrons. Additionally, a Schottky barrier with an additional depletion layer is created, resulting in a greater shift in the sensor's resistance. This sensor demonstrated excellent sensitivity and stability with a response of 11.12–100 ppm ethanol and the ability to detect 20 ppm acetone. The construction of hollow nanostructures and heterojunctions are effective measures to improve the performance of ternary metal oxide materials.

4. MOS E-nose for disease diagnosing

4.1. Cancer

Malignant tumors show a high morbidity and mortality rate in the twenty-first century. Cancer patients have the potential to be cured when the cancer is detected early and treated appropriately. MOS E-noses can fit the urgent need for mass and early cancer screening, allowing doctors to detect and treat patients earlier, and thus increasing the survival rates of patients.

Marzorati et al. [107] utilized a MOS E-nose to diagnose early-stage lung cancer. The sensor array produced 45 features, and these features were selected by sequential forward feature selection (SFFS) for specific diagnosis along with the patient's clinical features. With a discrimination sensitivity of 78% and 71%, respectively, the SVM classification model successfully distinguished lung cancer stage 1 patients, lung cancer stage 2–3 patients, and controls. This experiment pointed out that the baseline of the MOS sensor would change due to the environment and the drift of the sensor, which would affect the accuracy of the E-nose. Kononov et al. [108] installed an additional pump in the E-nose for cleaning the pipeline, allowing the study to obtain a baseline without signal drift. Three gases (heptane, ethylbenzene, and 1-propano) that could be lung cancer markers were used to optimize the measurement parameters. E-nose showed a good linear response for all these gases. The accuracy of the various classification models used (SVM, LDA, RF, KNN, and Logistic regression) was greater than 90%. With a correct identification rate of 97.2%, the logistic regression model had the best generalization for identifying lung cancer patients. Yan et al. [109] combined a-Fe_2O_3 and $ZnFe_2O_4$ by constructing n-n heterojunction. As shown in Fig. 7, this sensor showed a high response to 1 ppm n-butanol and exhibited good selectivity. It was also insensitive to humidity. The heterojunction structure can increase oxygen vacancies and produce more gas adsorption sites, which is expected to improve the performance of MOS E-noses.

To avoid other factors influencing VOCs, the control and patient groups need to have similar characteristics. Waltman et al. [110] chose urological patients and patients with prostatic hypertrophy (PE) as controls because their characteristics were similar to those of patients with prostate cancer (PCa). The ages of the subjects did not differ significantly. The PCa group had higher levels of prostate specific antigen (PSA) and significantly lower prostate volume. ANN model successfully differentiated prostate cancer patients. However, the sample size for this study is small and more data is needed to train the model. Taverna et al. [111] selected 174 subjects (88 PCa patients, 86 controls) for diagnosis using a MOS E-nose. Unlike the previous experiment which used exhaled breath as a sample, this experiment used the subject's urine headspace as a sample. This E-nose significantly differentiated the samples from the PCa and control groups. RF model distinguished PCa patients with 82.1% accuracy. This suggests that E-nose can discriminate against patients with PCa.

Giro Benet et al. [112] first distinguished the Breast cancer (BC) group from the control group with 92.31% accuracy using GC-MS techniques and Convolutional Neural Networks (CNN) models to demonstrate that their urine samples were significantly different. After training, the accuracy of MOS E-nose in identifying BC increased from 58.3% to 75%. Interestingly, the high average molecular weight of 8-oxodG (283.2407), one of the most reliable BC markers, may lead to its low concentration in the urine headspace. This provides a direction for later studies: improvements in heating methods and the sensitivity of gas sensors may enhance the accuracy of E-noses.

In summary, MOS E-nose has sufficient sensitivity to identify changes in VOCs in cancer patients. As the sample size increases, more data can be used to train E-nose's classification model, which will significantly improve the accuracy of E-nose.

4.2. Respiratory diseases

Van Velzen et al. [36] combined four E-noses, including a MOS E-nose, to form an E-nose platform for diagnosing chronic obstructive pulmonary disease (COPD). The thermolysis tubes and Tedlar bags were used for sampling in the experiment. GC-MS was used to identify ten COPD marker VOCs, including acetone, 1,2-pentadiene, toluene,

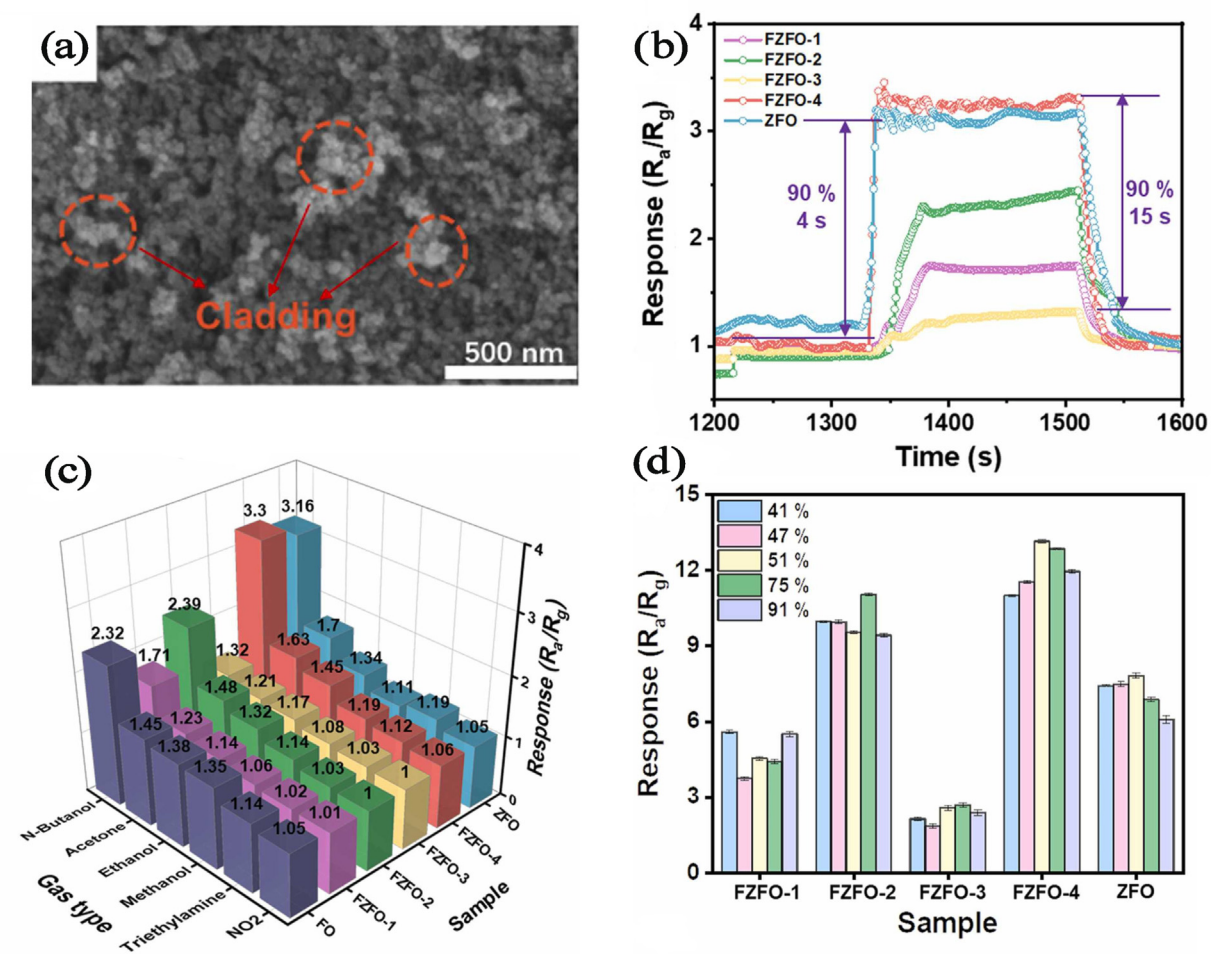

Fig. 7. (a) SEM images of FZFO-4; (b) Gas-sensing response curves to 1 ppm N-butanol; (c) Selectivity of the samples; (d) Responses of sensors at different RH to 10 ppm N-butanol [109].

butyrolactone, and others. E-nose successfully distinguished COPD patients in various stages with over 70% accuracy. However, the differences in VOCs found between patients with stable and worsening COPD in this trial were different from a previous study. Pizzini et al. [113] concluded that stable and deteriorating COPD could be distinguished by n-butane and others. The differences in these studies were attributed to the lack of standardization of experimental methods (design of study methods, severity of COPD in selected patients). Most patients with COPD and lung cancer have a smoking history, and smoking alters the VOCs in exhaled breath [114,115]. V.A. et al. [57] used a MOS E-nose to differentiate COPD from lung cancer patients. Over 70% of the testers had a history of smoking, and all testers were instructed to avoid eating and smoking for 2 h before testing. As shown in Fig. 8, the response of the sensor array showed significant differences between COPD patients and the healthy group. The XGBoost algorithm used in this study outperformed AdaBoost and Random Forest in terms of classification accuracy and avoided overfitting. At the validation stage, this E-nose differentiated COPD patients with 76.67% accuracy.

Intubated and mechanically ventilated critically ill patients have an 80% probability of contracting ventilator associated pneumonia (VAP) due to respiratory bacterial infections [116]. The MOS E-nose used by Schnabel et al. [117] had a sensitivity of 95% to detect VAP, but the specificity of this E-nose was only 38%. This was due to the mixing of dead zone gas when the gas was collected into the Tedlar bag, resulting in a low concentration of VOCs and an insufficient response of the MOS sensors. Liao et al. [118] used an E-nose to diagnose VAP in intensive care unit (ICU) patients. The MOS sensors in this E-nose were composed of reactive materials (ZnO_2, WO_3, etc.) and catalysts (gold, tungsten, etc.). The E-nose was calibrated before use to confirm that the response curve was within tolerance. The flow rate, humidity, and temperature were controlled within a certain range during the test. Under these conditions, SVM outperformed ANN in classification accuracy (92.08%). However, due to its higher nonlinear mapping, ANN could surpass SVM as the sample size increased. The E-nose is compact and convenient to be installed in the system of ICU and is suitable for detecting VAP.

Tuberculosis (TB) diagnosis in remote areas has always been a tricky problem. Mohamed et al. [119] utilized a MOS E-nose coupled with the PCA technique to detect headspace volatiles in TB patients' blood, breath, sputum, and urine. PCA clustering plots showed significant differences for all four samples, especially for blood and urine samples. Ultimately, the E-nose identified TB patients with an overall sensitivity of 98%. Coronel Teixeira et al. [120] used a handheld E-nose to diagnose tuberculosis. This subject included TB patients, asthma and COPD patients, and healthy people. Because of obesity, bronchitis, or antibiotics, some subjects were misclassified. The sensitivity of the ANN model to distinguish TB in the calibration stage reached 91%. This study was conducted in a hospital setting. However the team thought factors such as genetics and food could affect the smell print of TB patients in each region, so they conducted in-depth research on Paraguay's indigenous population [121]. The results showed that the completed ANN model's blind prediction specificity after training was 99%. In Hendrick's study, the accuracy of the E-nose using ANN was also 94.87% [122]. Expensive medical tests are impractical in remote areas. The E-nose can diagnose TB with only 5 min of exhalation, which is a good means of triage.

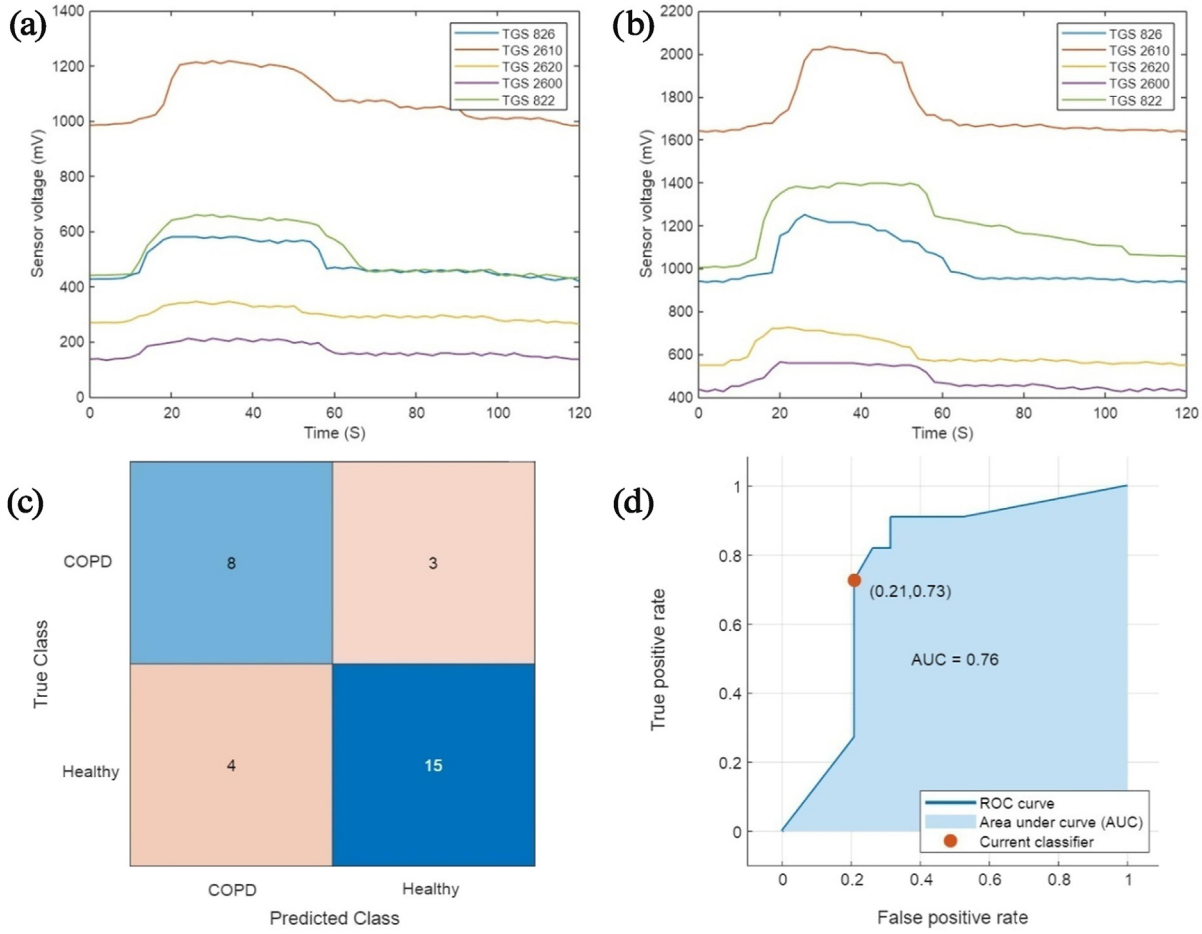

Fig. 8. Sensor array response to (a) a healthy control; (b) a COPD patient group; COPD detection with XGBoost in validation phase (c) confusion matrix; (d) ROC curve [57].

E-noses show high accuracy in diagnosing lung diseases. Providing a stable baseline, calibrating the E-nose, and increasing the number of sensors can provide better diagnostic results.

5. Summary and outlook

In the design process of the electronic nose, high performance sensors have been obtained through shape control, doping, and synthesis of composite materials. These sensors are rigorously calibrated and tested and then used to compose the electronic nose. E-noses consisting of MOS gas sensors have been successfully used to detect cancer and respiratory diseases. Current research has shown that the MOS E-nose provides rapid and accurate screening with good medical sensitivity and specificity even when patients do not have obvious symptoms. Some anticipated research trends and directions include:

(1) The sensitivity of MOS sensors to exhaled VOCs has been significantly improved, but the selectivity for specific gases requires in-depth study. Nanotechnology can be used to control particle properties, construct composite materials, and build heterojunctions to create synergistic effects, and significantly improve the selectivity of MOS gas sensors. Investigating the principles of the reaction process between gases and sensing materials can also help investigate new ways to improve sensor selectivity.

(2) The classification capability of E-nose can be significantly enhanced by boosting the feature extraction methods and classification model algorithm. In addition to the commonly used manual feature extraction (extraction of time-domain or frequency-domain features), features extracted by neural networks (such as autoencoders and deep confidence networks) are more distinguishable compared to traditional methods.

(3) Experiments on E-noses require a standardized test method, including gas collection, requirements for patients to abstain from food or smoke, etc., making the studies reproducible and comparable. And it must be tested with a larger sample size before clinical mass application. In clinical use, E-noses also need to overcome the effects of humidity, temperature, environmental VOCs, etc.

Declaration of competing interest

The authors declare that they have no known competing financial interests or personal relationships that could have appeared to influence the work reported in this paper.

Acknowledgments

This work is supported by the Outstanding Youth Foundation of Jiangsu Province of China (No. BK20211548), the Yangzhou Science and Technology Plan Project (YZ2023246).

References

[1] R. Einoch Amor, A. Zinger, Y.Y. Broza, A. Schroeder, H. Haick, Artificially intelligent nanoarray detects various cancers by liquid biopsy of volatile markers, Adv. Healthcare Mater. 11 (2022) 2200356, https://doi.org/10.1002/adhm.202200356.

[2] S. Das, M. Pal, Review—non-invasive monitoring of human health by exhaled breath analysis: a comprehensive review, J. Electrochem. Soc. 167 (2020) 037562, https://doi.org/10.1149/1945-7111/ab67a6.
[3] L. Pauling, A.B. Robinson, R. Teranishi, P. Cary, Quantitative analysis of urine vapor and breath by gas-liquid partition chromatography, Proc. Natl. Acad. Sci. U.S.A. 68 (1971) 2374–2376, https://doi.org/10.1073/pnas.68.10.2374.
[4] H. Haick, Y.Y. Broza, P. Mochalski, V. Ruzsanyi, A. Amann, Assessment, origin, and implementation of breath volatile cancer markers, Chem. Soc. Rev. 43 (2014) 1423–1449, https://doi.org/10.1039/c3cs60329f.
[5] M. Phillips, K. Gleeson, J.M.B. Hughes, J. Greenberg, R.N. Cataneo, L. Baker, W.P. McVay, Volatile organic compounds in breath as markers of lung cancer: a cross-sectional study, Lancet 353 (1999) 1930–1933, https://doi.org/10.1016/S0140-6736(98)07552-7.
[6] Q. Yang, B.H. Shi, G.L. Tian, Q.Q. Niu, J. Tang, D.D. Linghu, H.Q. He, B.Q. Wu, J.T. Yang, L. Xu, R.Q. Yu, GC-MS urinary metabolomics analysis of inherited metabolic diseases and stable metabolic biomarker screening by a comprehensive chemometric method, Microchem. J. 168 (2021) 106350, https://doi.org/10.1016/j.microc.2021.106350.
[7] F. Monedeiro, R.B. dos Reis, F.M. Peria, C.T.G. Sares, B.S. De Martinis, Investigation of sweat VOC profiles in assessment of cancer biomarkers using HS-GC-MS, J. Breath Res. 14 (2020) 026009, https://doi.org/10.1088/1752-7163/ab5b3c.
[8] J.D. Pleil, A. Hansel, J. Beauchamp, Advances in proton transfer reaction mass spectrometry (PTR-MS): applications in exhaled breath analysis, food science, and atmospheric chemistry, J. Breath Res. 13 (2019) 039002, https://doi.org/10.1088/1752-7163/ab21a7.
[9] P. Španěl, D. Smith, Quantification of volatile metabolites in exhaled breath by selected ion flow tube mass spectrometry, SIFT-MS, Clin. Mass Spectrom. 16 (2020) 18–24, https://doi.org/10.1016/j.clinms.2020.02.001.
[10] R.W. Moncrieff, An instrument for measuring and classifying odors, J. Appl. Physiol. 16 (1961) 742–749, https://doi.org/10.1152/jappl.1961.16.4.742.
[11] W.F. Wilkens, J.D. Hartman, An electronic analog for the olfactory processes a, J. Food Sci. 29 (1964) 372–378, https://doi.org/10.1111/j.1365-2621.1964.tb01746.x.
[12] K. Persaud, G. Dodd, Analysis of discrimination mechanisms in the mammalian olfactory system using a model nose, Nature 299 (1982) 352–355, https://doi.org/10.1038/299352a0.
[13] J.W. Gardner, P.N. Bartlett, A brief history of electronic noses, Sens. Actuators, B 18 (1994) 210–211, https://doi.org/10.1016/0925-4005(94)87085-3.
[14] Y. Tang, X. Wang, Q. Zhang, Y. Li, H. Wang, Solvothermal synthesis of Co1−xNixFe2O4 nanoparticles and its application in ammonia vapors detection, Prog. Nat. Sci.: Mater. Int. 22 (2012) 53–58, https://doi.org/10.1016/j.pnsc.2011.12.009.
[15] X. He, H. Chai, Y. Luo, L. Min, M. Debliquy, C. Zhang, Metal oxide semiconductor gas sensing materials for early lung cancer diagnosis, J. Adv. Ceram. 12 (2023) 207–227, https://doi.org/10.26599/JAC.2023.9220694.
[16] Y. Wei, X. Wang, G. Yi, L. Zhou, J. Cao, G. Sun, Z. Chen, H. Bala, Z. Zhang, Hydrothermal synthesis of Ag modified ZnO nanorods and their enhanced ethanol-sensing properties, Mater. Sci. Semicond. Process. 75 (2018) 327–333, https://doi.org/10.1016/j.mssp.2017.11.007.
[17] G. Meng, F. Zhuge, K. Nagashima, A. Nakao, M. Kanai, Y. He, M. Boudot, T. Takahashi, K. Uchida, T. Yanagida, Nanoscale thermal management of single SnO2 nanowire: pico-oule energy consumed molecule sensor, ACS Sens. 1 (2016) 997–1002, https://doi.org/10.1021/acssensors.6b00364.
[18] S. Dragonieri, G. Pennazza, P. Carratu, O. Resta, Electronic nose technology in respiratory diseases, Lung 195 (2017) 157–165, https://doi.org/10.1007/s00408-017-9987-3.
[19] A.D. Wilson, Application of electronic-nose technologies and VOC-biomarkers for the noninvasive early diagnosis of gastrointestinal diseases, Sensors 18 (2018) 2613, https://doi.org/10.3390/s18082613.
[20] S. Lekha, M. S, Recent advancements and future prospects on E-nose sensors technology and machine learning approaches for non-invasive diabetes diagnosis: a review, IEEE Rev. Biomed. Eng. 14 (2021) 127–138, https://doi.org/10.1109/RBME.2020.2993591.
[21] S. Scarlata, P. Finamore, M. Meszaros, S. Dragonieri, A. Bikov, The role of electronic noses in phenotyping patients with chronic obstructive pulmonary disease, Biosensors 10 (2020) 171, https://doi.org/10.3390/bios10110171.
[22] W. Miekisch, J.K. Schubert, G.F.E. Noeldge-Schomburg, Diagnostic potential of breath analysis—focus on volatile organic compounds, Clin. Chim. Acta 347 (2004) 25–39, https://doi.org/10.1016/j.cccn.2004.04.023.
[23] A.T. Guntner, S. Abegg, K. Konigstein, P.A. Gerber, A. Schmidt-Trucksass, S.E. Pratsinis, Breath sensors for health monitoring, ACS Sens. 4 (2019) 268–280, https://doi.org/10.1021/acssensors.8b00937.
[24] P.A. Kirkham, P.J. Barnes, Oxidative stress in COPD, Chest 144 (2013) 266–273, https://doi.org/10.1378/chest.12-2664.
[25] A. Ramond, D. Godin-Ribuot, C. Ribuot, P. Totoson, I. Koritchneva, S. Cachot, P. Levy, M. Joyeux-Faure, Oxidative stress mediates cardiac infarction aggravation induced by intermittent hypoxia, Fundam. Clin. Pharmacol. 27 (2013) 252–261, https://doi.org/10.1111/j.1472-8206.2011.01015.x.
[26] M. Kinter, Analytical technologies for lipid oxidation products analysis, J. Chromatogr. A 671 (1995) 223–236, https://doi.org/10.1016/0378-4347(95)00189-.
[27] A. Azim, C. Barber, P. Dennison, J. Riley, P. Howarth, Exhaled volatile organic compounds in adult asthma: a systematic review, Eur. Respir. J. 54 (2019) 1900056, https://doi.org/10.1183/13993003.00056-2019.
[28] F. Monedeiro, M. Monedeiro-Milanowski, I.-A. Ratiu, B. Brożek, T. Ligor, B. Buszewski, Needle trap device-GC-MS for characterization of lung diseases based on breath VOC profiles, Molecules 26 (2021) 1789, https://doi.org/10.3390/molecules26061789.
[29] P. Puchalska, P.A. Crawford, Multi-dimensional roles of ketone bodies in fuel metabolism, signaling, and therapeutics, Cell Metabol. 25 (2017) 262–284, https://doi.org/10.1016/j.cmet.2016.12.022.
[30] O. Alkedeh, R. Priefer, The ketogenic diet: breath acetone sensing technology, Biosensors 11 (2021) 26, https://doi.org/10.3390/bios11010026.
[31] M. Shokrekhodaei, S. Quinones, Review of non-invasive glucose sensing techniques: optical, electrical and breath acetone, Sensors 20 (2020) 1251, https://doi.org/10.3390/s20051251.
[32] Z. Jia, H. Zhang, C.N. Ong, A. Patra, Y. Lu, C.T. Lim, T. Venkatesan, Detection of lung cancer: concomitant volatile organic compounds and metabolomic profiling of six cancer cell lines of different histological origins, ACS Omega 3 (2018) 5131–5140, https://doi.org/10.1021/acsomega.7b02035.
[33] A.R. Lima, J. Pinto, A.I. Azevedo, D. Barros-Silva, C. Jerónimo, R. Henrique, M. de Lourdes Bastos, P. Guedes de Pinho, M. Carvalho, Identification of a biomarker panel for improvement of prostate cancer diagnosis by volatile metabolic profiling of urine, Br. J. Cancer 121 (2019) 857–868, https://doi.org/10.1038/s41416-019-0585-4.
[34] M. Phillips, R.N. Cataneo, C. Saunders, P. Hope, P. Schmitt, J. Wai, Volatile biomarkers in the breath of women with breast cancer, J. Breath Res. 4 (2010) 026003, https://doi.org/10.1088/1752-7155/4/2/026003.
[35] Y. Zhang, G. Gao, H. Liu, H. Fu, J. Fan, K. Wang, Y. Chen, B. Li, C. Zhang, X. Zhi, L. He, D. Cui, Identification of volatile biomarkers of gastric cancer cells and ultrasensitive electrochemical detection based on sensing interface of Au-Ag alloy coated MWCNTs, Theranostics 4 (2014) 154–162, https://doi.org/10.7150/thno.7560.
[36] P. Van Velzen, P. Brinkman, H.H. Knobel, J.W.K. van den Berg, R.E. Jonkers, R.J. Loijmans, J.M. Prins, P.J. Sterk, Exhaled breath profiles before, during and after exacerbation of COPD: a prospective follow-up study, COPD 16 (2019) 330–337, https://doi.org/10.1080/15412555.2019.1669550.
[37] M. Phillips, R.N. Cataneo, R. Condos, G.A. Ring Erickson, J. Greenberg, V. La Bombardi, M.I. Munawar, O. Tietje, Volatile biomarkers of pulmonary tuberculosis in the breath, Tuberculosis 87 (2007) 44–52, https://doi.org/10.1016/j.tube.2006.03.004.
[38] D.M. Ruszkiewicz, D. Sanders, R. O'Brien, F. Hempel, M.J. Reed, A.C. Riepe, K. Bailie, E. Brodrick, K. Darnley, R. Ellerkmann, O. Mueller, A. Skarysz, M. Truss, T. Wortelmann, S. Yordanov, C.L.P. Thomas, B. Schaaf, M. Eddleston, Diagnosis of COVID-19 by analysis of breath with gas chromatography-ion mobility spectrometry - a feasibility study, EClinicalMedicine 29–30 (2020) 100609, https://doi.org/10.1016/j.eclinm.2020.100609.
[39] H. Chen, X. Qi, L. Zhang, X. Li, J. Ma, C. Zhang, H. Feng, M. Yao, COVID-19 screening using breath-borne volatile organic compounds, J. Breath Res. 15 (2021) 047104, https://doi.org/10.1088/1752-7163/ac2e57.
[40] P. Trefz, J. Obermeier, R. Lehbrink, J.K. Schubert, W. Miekisch, D.-C. Fischer, Exhaled volatile substances in children suffering from type 1 diabetes mellitus: results from a cross-sectional study, Sci. Rep. 9 (2019) 15707, https://doi.org/10.1038/s41598-019-52165-x.
[41] J. Herbig, T. Titzmann, J. Beauchamp, I. Kohl, A. Hansel, Buffered end-tidal (BET) sampling—a novel method for real-time breath-gas analysis, J. Breath Res. 2 (2008) 037008, https://doi.org/10.1088/1752-7155/2/3/037008.
[42] T. Liu, W. Zhang, L. Ye, M. Ueland, S.L. Forbes, S.W. Su, A novel multi-odour identification by electronic nose using non-parametric modelling-based feature extraction and time-series classification, Sens. Actuators, B 298 (2019) 126690, https://doi.org/10.1016/j.snb.2019.126690.
[43] F. Raspagliesi, G. Bogani, S. Benedetti, S. Grassi, S. Ferla, S. Buratti, Detection of ovarian cancer through exhaled breath by electronic nose: a prospective study, Cancers 12 (2020) 2408, https://doi.org/10.3390/cancers12092408.
[44] P. Bassi, L. Di Gianfrancesco, L. Salmaso, M. Ragonese, G. Palermo, E. Sacco, R.A. Giancristofaro, R. Ceccato, M. Racioppi, Improved non-invasive diagnosis of bladder cancer with an electronic nose: a large pilot study, J. Clin. Med. 10 (2021) 4984, https://doi.org/10.3390/jcm10214984.
[45] K. Liu, C. Zhang, Volatile organic compounds gas sensor based on quartz crystal microbalance for fruit freshness detection: a review, Food Chem. 334 (2021) 127615, https://doi.org/10.1016/j.foodchem.2020.127615.
[46] N.M. Zetola, C. Modongo, O. Matsiri, T. Tamuhla, B. Mbongwe, K. Matlhagela, E. Sepako, A. Catini, G. Sirugo, E. Martinelli, R. Paolesse, C. Di Natale, Diagnosis of pulmonary tuberculosis and assessment of treatment response through analyses of volatile compound patterns in exhaled breath samples, J. Infect. 74 (2017) 367–376, https://doi.org/10.1016/j.jinf.2016.12.006.
[47] V. Nagarajan, R. Chandiramouli, DFT investigation of NH3 gas interactions on TeO2 nanostructures, Prog. Nat. Sci.: Mater. Int. 26 (2016) 129–138, https://doi.org/10.1016/j.pnsc.2016.03.010.
[48] A.T. Guntner, V. Koren, K. Chikkadi, M. Righettoni, S.E. Pratsinis, E-nose sensing of low-ppb formaldehyde in gas mixtures at high relative humidity for breath screening of lung cancer? ACS Sens. 1 (2016) 528–535, https://doi.org/10.1021/acssensors.6b00008.
[49] D. Zhang, Z. Yang, S. Yu, Q. Mi, Q. Pan, Diversiform metal oxide-based hybrid nanostructures for gas sensing with versatile prospects, Coord. Chem. Rev. 413 (2020) 213272, https://doi.org/10.1016/j.ccr.2020.213272.
[50] K. Zhang, J. Wang, T. Liu, Y. Luo, X.J. Loh, X. Chen, Machine learning-reinforced noninvasive biosensors for healthcare, Adv. Healthcare Mater. 10 (2021) 2100734, https://doi.org/10.1002/adhm.202100734.

[51] C. Wongchoosuk, M. Lutz, T. Kerdcharoen, Detection and classification of human body odor using an electronic nose, Sensors 9 (2009) 7234–7249, https://doi.org/10.3390/s90907234.
[52] K. Polat, S. Güneş, Computer aided medical diagnosis system based on principal component analysis and artificial immune recognition system classifier algorithm, Expert Syst. Appl. 34 (2008) 773–779, https://doi.org/10.1016/j.eswa.2006.10.011.
[53] G. Kerschen, J.C. Golinval, Non-linear generalization of principal component analysis: from a global to a local approach, J. Sound Vib. 254 (2002) 867–876, https://doi.org/10.1006/jsvi.2001.4129.
[54] O.I. Abiodun, A. Jantan, A.E. Omolara, K.V. Dada, A.M. Umar, O.U. Linus, H. Arshad, A.A. Kazaure, U. Gana, M.U. Kiru, Comprehensive review of artificial neural network applications to pattern recognition, IEEE Access 7 (2019) 158820–158846, https://doi.org/10.1109/ACCESS.2019.2945545.
[55] R.M.G.E. van de Goor, J.C.A. Hardy, M.R.A. van Hooren, B. Kremer, K.W. Kross, Detecting recurrent head and neck cancer using electronic nose technology: a feasibility study, Head Neck 41 (2019) 2983–2990, https://doi.org/10.1002/hed.25787.
[56] T. Saidi, O. Zaim, M. Moufid, N. El Bari, R. Ionescu, B. Bouchikhi, Exhaled breath analysis using electronic nose and gas chromatography–mass spectrometry for non-invasive diagnosis of chronic kidney disease, diabetes mellitus and healthy subjects, Sens. Actuators, B 257 (2018) 178–188, https://doi.org/10.1016/j.snb.2017.10.178.
[57] V.A. B, M. Subramoniam, L. Mathew, Detection of COPD and Lung Cancer with electronic nose using ensemble learning methods, Clin. Chim. Acta 523 (2021) 231–238, https://doi.org/10.1016/j.cca.2021.10.005.
[58] A. De Vincentis, G. Pennazza, M. Santonico, U. Vespasiani-Gentilucci, G. Galati, P. Gallo, C. Vernile, C. Pedone, R. Antonelli Incalzi, A. Picardi, Breath-print analysis by e-nose for classifying and monitoring chronic liver disease: a proof-of-concept study, Sci. Rep. 6 (2016) 25337, https://doi.org/10.1038/srep25337.
[59] T.G. de Meij, I.B. Larbi, M.P. van der Schee, Y.E. Lentferink, T. Paff, J.S. Terhaar sive Droste, C.J. Mulder, A.A. van Bodegraven, N.K. de Boer, Electronic nose can discriminate colorectal carcinoma and advanced adenomas by fecal volatile biomarker analysis: proof of principle study, Int. J. Cancer 134 (2014) 1132–1138, https://doi.org/10.1002/ijc.28446.
[60] M. Tirzïte, M. Bukovskis, G. Strazda, N. Jurka, I. Taivans, Detection of lung cancer with electronic nose and logistic regression analysis, J. Breath Res. 13 (2019) 016006, https://doi.org/10.1088/1752-7163/aae1b8.
[61] X. Kuang, T. Liu, D. Shi, W. Wang, M. Yang, S. Hussain, X. Peng, F. Pan, Hydrothermal synthesis of hierarchical SnO2 nanostructures made of superfine nanorods for smart gas sensor, Appl. Surf. Sci. 364 (2016) 371–377, https://doi.org/10.1016/j.apsusc.2015.12.172.
[62] P.G. Choi, N. Shirahata, Y. Masuda, Tin oxide nanosheet thin film with bridge type structure for gas sensing, Thin Solid Films 698 (2020) 137845, https://doi.org/10.1016/j.tsf.2020.137845.
[63] V. Saasa, B. Mwakikunga, Facile synthesis, characterization and acetone sensing properties of n-type WO3, SnO2 and VO2 semiconducting materials and their cobalt doped performance: Outstanding SnO2-Co acetone selectivity and sensitivity, Mater. Res. Bull. 164 (2023) 112288, https://doi.org/10.1016/j.materresbull.2023.112288.
[64] N. Van Duy, D.T.T. Trang, D.T.T. Le, C.M. Hung, M. Tonezzer, H. Nguyen, N.D. Hoa, Enhancement of NH3 gas sensing with Ag-Pt co-catalyst on SnO2 nanofilm towards medical diagnosis, Thin Solid Films 767 (2023) 139682, https://doi.org/10.1016/j.tsf.2023.139682.
[65] M. Narjinary, P. Rana, A. Sen, M. Pal, Enhanced and selective acetone sensing properties of SnO2-MWCNT nanocomposites: promising materials for diabetes sensor, Mater. Des. 115 (2017) 158–164, https://doi.org/10.1016/j.matdes.2016.11.042.
[66] G. Marappan, R. Kalidoss, V.J. Surya, Y. Sivalingam, Elucidation of sensing mechanism through VOCs induced surface potential changes on graphene oxide/tin oxide nanocomposites, Ceram. Int. 48 (2022) 29152–29157, https://doi.org/10.1016/j.ceramint.2022.05.074.
[67] H. Benelmadjat, B. Boudine, A. Keffous, N. Gabouze, Photoresponse and H2 gas sensing properties of highly oriented Al and Al/Sb doped ZnO thin films, Prog. Nat. Sci.: Mater. Int. 23 (2013) 519–523, https://doi.org/10.1016/j.pnsc.2013.11.001.
[68] H. Bian, S. Ma, A. Sun, X. Xu, G. Yang, S. Yan, J. Gao, Z. Zhang, H. Zhu, Improvement of acetone gas sensing performance of ZnO nanoparticles, J. Alloys Compd. 658 (2016) 629–635, https://doi.org/10.1016/j.jallcom.2015.09.217.
[69] C. Zhang, Y. Li, G.-F. Liu, H.-L. Liao, Preparation of ZnO1-x by peroxide thermal decomposition and its room temperature gas sensing properties, Rare Met. 41 (2022) 871–876, https://doi.org/10.1007/s12598-021-01840-y.
[70] Y. Hou, A.H. Jayatissa, Influence of laser doping on nanocrystalline ZnO thin films gas sensors, Prog. Nat. Sci.: Mater. Int. 27 (2017) 435–442, https://doi.org/10.1016/j.pnsc.2017.07.002.
[71] R. Yoo, Y. Park, H. Jung, H.J. Rim, S. Cho, H.-S. Lee, W. Lee, Acetone-sensing properties of doped ZnO nanoparticles for breath-analyzer applications, J. Alloys Compd. 803 (2019) 135–144, https://doi.org/10.1016/j.jallcom.2019.06.254.
[72] C. Singh, E. Panda, Variation of electrical properties in thickening Al-doped ZnO films: role of defect chemistry, RSC Adv. 6 (2016) 48910–48918, https://doi.org/10.1039/c6ra06513a.
[73] L.H. Kathwate, G. Umadevi, P.M. Kulal, P. Nagaraju, D.P. Dubal, A.K. Nanjundan, V.D. Mote, Ammonia gas sensing properties of Al doped ZnO thin films, Sens. Actuators, A 313 (2020) 112193, https://doi.org/10.1016/j.sna.2020.112193.
[74] R. Sankar ganesh, M. Navaneethan, G.K. Mani, S. Ponnusamy, K. Tsuchiya, C. Muthamizhchelvan, S. Kawasaki, Y. Hayakawa, Influence of Al doping on the structural, morphological, optical, and gas sensing properties of ZnO nanorods, J. Alloys Compd. 698 (2017) 555–564, https://doi.org/10.1016/j.jallcom.2016.12.187.
[75] J. Zhang, X. Jia, T. Liu, J. Yang, S. Wang, Y. Li, D. Shao, L. Feng, H. Song, Cactus-inspired GO/ZnO sensors for fast and robust acetone sensing properties, Ceram. Int. 49 (2023) 5861–5871, https://doi.org/10.1016/j.ceramint.2022.10.210.
[76] S. Gupta, C. Ravikant, A. Kaur, One-pot wet chemical synthesis of reduced graphene oxide-zinc oxide nanocomposites for fast and selective ammonia sensing at room temperature, Sens. Actuators, A 331 (2021) 112965, https://doi.org/10.1016/j.sna.2021.112965.
[77] D. Zhang, W. Pan, L. Zhou, S. Yu, Room-temperature benzene sensing with Au-doped ZnO nanorods/exfoliated WSe2 nanosheets and density functional theory simulations, ACS Appl. Mater. Interfaces 13 (2021) 33392–33403, https://doi.org/10.1021/acsami.1c03884.
[78] F. Ma, B. Yang, Z. Zhang, J. Kong, G. Huang, Y. Mei, Self-rolled TiO2 microscroll/graphene composite for electrochemical dopamine sensing, Prog. Nat. Sci.: Mater. Int. 30 (2020) 337–342, https://doi.org/10.1016/j.pnsc.2020.02.008.
[79] Y. Kimura, S. Kimura, R. Kojima, M. Bitoh, M. Abe, M. Niwano, Micro-scaled hydrogen gas sensors with patterned anodic titanium oxide nanotube film, Sens. Actuators, B 177 (2013) 1156–1160, https://doi.org/10.1016/j.snb.2012.12.016.
[80] H. Abe, Y. Kimura, T. Ma, D. Tadaki, A. Hirano-Iwata, M. Niwano, Response characteristics of a highly sensitive gas sensor using a titanium oxide nanotube film decorated with platinum nanoparticles, Sens. Actuators, B 321 (2020) 128525, https://doi.org/10.1016/j.snb.2020.128525.
[81] K. Iwata, H. Abe, T. Ma, D. Tadaki, A. Hirano-Iwata, Y. Kimura, S. Suda, M. Niwano, Application of neural network based regression model to gas concentration analysis of TiO2 nanotube-type gas sensors, Sens. Actuators, B 361 (2022) 131732, https://doi.org/10.1016/j.snb.2022.131732.
[82] M. Yin, Z. Zhu, Mesoporous NiO as an ultra-highly sensitive and selective gas sensor for sensing of trace ammonia at room temperature, J. Alloys Compd. 789 (2019) 941–947, https://doi.org/10.1016/j.jallcom.2019.03.143.
[83] Y. Liu, J. Bai, Y. Li, L. Yang, Y. Wang, Y. Li, F. Liu, Y. Zhang, G. Lu, Preparation of PdO-decorated NiO porous film on ceramic substrate for highly selective and sensitive H2S detection, Ceram. Int. 48 (2022) 4787–4794, https://doi.org/10.1016/j.ceramint.2021.11.015.
[84] L. Zhu, W. Zeng, J. Yang, Y. Li, One-step hydrothermal fabrication of nanosheet-assembled NiO/ZnO microflower and its ethanol sensing property, Ceram. Int. 44 (2018) 19825–19830, https://doi.org/10.1016/j.ceramint.2018.07.240.
[85] M. Tang, D. Zhang, Q. Chen, Z. Wang, D. Wang, Z. Yang, W. Xu, L. Wang, L. Zhu, F. An, Heterostructure construction of SnS2 Debye nanowires modified with ZnO nanorods for chemiresistive H2S detection in sulfur hexafluoride decomposition products, Sens. Actuators, B 390 (2023) 133952, https://doi.org/10.1016/j.snb.2023.133952.
[86] C. Zhang, Y. Huan, Y. Li, Y. Luo, M. Debliquy, Low concentration isopropanol gas sensing properties of Ag nanoparticles decorated In2O3 hollow spheres, J. Adv. Ceram. 11 (2022) 379–391, https://doi.org/10.1007/s40145-021-0530-x.
[87] C. Zhang, D. Sun, Y. Huan, K. Wu, H. Liao, Highly sensitive ZnO nanoparticles-loaded In2O3 hollow microsphere for detecting ppb-level NO2 at low working temperature, Prog. Nat. Sci.: Mater. Int. 30 (2020) 469–476, https://doi.org/10.1016/j.pnsc.2020.06.006.
[88] B. Han, H. Wang, W. Yang, J. Wang, X. Wei, Hierarchical Pt-decorated In2O3 microspheres with highly enhanced isoprene sensing properties, Ceram. Int. 47 (2021) 9477–9485, https://doi.org/10.1016/j.ceramint.2020.12.081.
[89] M. Punginsang, D. Zappa, E. Comini, A. Wisitsoraat, G. Sberveglieri, A. Ponzoni, C. Liewhiran, Selective H2S gas sensors based on ohmic hetero-interface of Au-functionalized WO3 nanowires, Appl. Surf. Sci. 571 (2022) 151262, https://doi.org/10.1016/j.apsusc.2021.151262.
[90] M. Kumaresan, M. Venkatachalam, M. Saroja, P. Gowthaman, TiO2 nanofibers decorated with monodispersed WO3 heterostruture sensors for high gas sensing performance towards H2 gas, Inorg. Chem. Commun. 129 (2021) 108663, https://doi.org/10.1016/j.inoche.2021.108663.
[91] D. Zhang, Q. Mi, D. Wang, T. Li, MXene/Co3O4 composite based formaldehyde sensor driven by ZnO/MXene nanowire arrays piezoelectric nanogenerator, Sens. Actuators, B 339 (2021) 129923, https://doi.org/10.1016/j.snb.2021.129923.
[92] J. Wang, S. Jiang, H. Liu, S. Wang, Q. Pan, Y. Yin, G. Zhang, P- type gas-sensing behavior of Ga2O3/Al2O3 nanocomposite with high sensitivity to NOx at room temperature, J. Alloys Compd. 814 (2020) 152284, https://doi.org/10.1016/j.jallcom.2019.152284.
[93] U. Nakate, Y.-T. Yu, S. Park, Hierarchical CuO nanostructured materials for acetaldehyde sensor application, Microelectron. Eng. 251 (2022) 111662, https://doi.org/10.1016/j.mee.2021.111662.
[94] N. Roy, R. Sinha, H.B. Nemade, T.K. Mandal, Synthesis of MoS2-CuO nanocomposite for room temperature acetone sensing application, J. Alloys Compd. 910 (2022) 164891, https://doi.org/10.1016/j.jallcom.2022.164891.
[95] F. Meng, Z. Yang, Z. Yuan, H. Zhang, H. Zhu, Hydrothermal synthesis of CuO/rGO nanosheets for enhanced gas sensing properties of ethanol, Ceram. Int. 49 (2023) 5595–5603, https://doi.org/10.1016/j.ceramint.2022.10.174.
[96] H. Bai, H. Guo, J. Wang, Y. Dong, B. Liu, Z. Xie, F. Guo, D. Chen, R. Zhang, Y. Zheng, A room-temperature NO2 gas sensor based on CuO nanoflakes modified with rGO nanosheets, Sens. Actuators, B 337 (2021) 129783, https://doi.org/10.1016/j.snb.2021.129783.
[97] M. Dun, M. Tang, D. Zhao, X. Li, X. Huang, Synergistic effect of PdO and parallel nanowires assembled CuO microspheres enables high performance room-temperature H2S sensor, Sens. Actuators, B 358 (2022) 131520, https://doi.org/10.1016/j.snb.2022.131520.

[98] T.K. Dang, N.D. Cuong, H. Van Minh Hai, T.Q. Phuong, L.L. Son, D. Thi Thanh Nhan, V. Van Tan, M.D. Hien, K.-J. Jeon, N.Q. Hung, L.A. Tuyen, N. Van Hieu, Exploring novel p-n core/shell structure in single α-Fe2O3 nanorods of hierarchical hollow microspheres for ultrasensitive acetone gas sensor, Sens. Actuators, B 383 (2023) 133573, https://doi.org/10.1016/j.snb.2023.133573.

[99] Z. Lei, P. Cheng, Y. Wang, L. Xu, L. Lv, X. Li, S. Sun, X. Hao, Y. Zhang, Y. Zhang, Z. Weng, Pt-doped α-Fe2O3 mesoporous microspheres with low-temperature ultra-sensitive properties for gas sensors in diabetes detection, Appl. Surf. Sci. 607 (2023) 154558, https://doi.org/10.1016/j.apsusc.2022.154558.

[100] B. Zhang, N. Bao, T. Wang, Y. Xu, Y. Dong, Y. Ni, P. Yu, Q. Wei, J. Wang, L. Guo, Y. Xia, High-performance room temperature NO2 gas sensor based on visible light irradiated In2O3 nanowires, J. Alloys Compd. 867 (2021) 159076, https://doi.org/10.1016/j.jallcom.2021.159076.

[101] D. Zhang, J. Wu, Y. Cao, Cobalt-doped indium oxide/molybdenum disulfide ternary nanocomposite toward carbon monoxide gas sensing, J. Alloys Compd. 777 (2019) 443–453, https://doi.org/10.1016/j.jallcom.2018.10.365.

[102] S. Mehmood, X. Zhao, M. Fahad Bhopal, F. Ullah Khan, Y. Yang, G. Wang, X. Pan, MoO2-Ni-graphene ternary nanocomposite for a high- performance room-temperature ethanol gas sensor, Appl. Surf. Sci. 554 (2021) 149595, https://doi.org/10.1016/j.apsusc.2021.149595.

[103] N.H. Hanh, T.M. Ngoc, L. Van Duy, C.M. Hung, N. Van Duy, N.D. Hoa, A comparative study on the VOCs gas sensing properties of Zn2SnO4 nanoparticles, hollow cubes, and hollow octahedra towards exhaled breath analysis, Sens. Actuators, B 343 (2021) 130147, https://doi.org/10.1016/j.snb.2021.130147.

[104] K.-D. Wu, J.-Y. Xu, M. Debliquy, C. Zhang, Synthesis and NH3/TMA sensing properties of CuFe2O4 hollow microspheres at low working temperature, Rare Met. 40 (2021) 1768–1777, https://doi.org/10.1007/s12598-020-01609-9.

[105] D. Rathore, S. Mitra, R. Kurchania, R.K. Pandey, Physicochemical properties of CuFe2O4 nanoparticles as a gas sensor, J. Mater. Sci. Mater. Electron. 29 (2018) 1925–1932, https://doi.org/10.1007/s10854-017-8102-0.

[106] D. Ma, L. Zhang, J. Hu, Z. Fu, T. Luo, D. Yang, D. Fang, J. Li, J. Peng, Y. Wang, Preparation and gas-sensitive properties of hollow Zn2SnO4/SnO2 nano-cubes, Inorg. Chem. Commun. 141 (2022) 109507, https://doi.org/10.1016/j.inoche.2022.109507.

[107] D. Marzorati, L. Mainardi, G. Sedda, R. Gasparri, L. Spaggiari, P. Cerveri, MOS sensors array for the discrimination of lung cancer and at-risk subjects with exhaled breath analysis, Chemosensors 9 (2021) 209, https://doi.org/10.3390/chemosensors9080209.

[108] A. Kononov, B. Korotetsky, I. Jahatspanian, A. Gubal, A. Vasiliev, A. Arsenjev, A. Nefedov, A. Barchuk, I. Gorbunov, K. Kozyrev, A. Rassadina, E. Iakovleva, M. Sillanpää, Z. Safaei, N. Ivanenko, N. Stolyarova, V. Chuchina, A. Ganeev, Online breath analysis using metal oxide semiconductor sensors (electronic nose) for diagnosis of lung cancer, J. Breath Res. 14 (2020) 016004, https://doi.org/10.1088/1752-7163/ab433d.

[109] W. Yan, W. Liu, Z. Zhao, J. Wang, G.B. Nam, S. Cui, X. Shen, H.W. Jang, Humidity-independent electronic nose of α-Fe2O3/ZnFe2O4 heterojunctions for trace detection of N-butanol exhalation in lung cancer screening, Sens. Actuators, B 384 (2023) 133577, https://doi.org/10.1016/j.snb.2023.133577.

[110] C.G. Waltman, T.A.T. Marcelissen, J.G.H. van Roermund, Exhaled-breath testing for prostate cancer based on volatile organic compound profiling using an electronic nose device (Aeonose™): a preliminary report, Eur. Urol. Focus 6 (2020) 1220–1225, https://doi.org/10.1016/j.euf.2018.11.006.

[111] G. Taverna, F. Grizzi, L. Tidu, C. Bax, M. Zanoni, P. Vota, B.J. Lotesoriere, S. Prudenza, L. Magagnin, G. Langfelder, N. Buffi, P. Casale, L. Capelli, Accuracy of a new electronic nose for prostate cancer diagnosis in urine samples, Int. J. Urol. 29 (2022) 890–896, https://doi.org/10.1111/iju.14912.

[112] J. Giró Benet, M. Seo, M. Khine, J. Gumà Padró, A. Pardo Martnez, F. Kurdahi, Breast cancer detection by analyzing the volatile organic compound (VOC) signature in human urine, Sci. Rep. 12 (2022) 14873, https://doi.org/10.1038/s41598-022-17795-8.

[113] A. Pizzini, W. Filipiak, J. Wille, C. Ager, H. Wiesenhofer, R. Kubinec, J. Blaško, C. Tschurtschenthaler, C.A. Mayhew, G. Weiss, R. Bellmann-Weiler, Analysis of volatile organic compounds in the breath of patients with stable or acute exacerbation of chronic obstructive pulmonary disease, J. Breath Res. 12 (2018) 036002, https://doi.org/10.1088/1752-7163/aaa4c5.

[114] N. Fens, A.H. Zwinderman, M.P. van der Schee, S.B. de Nijs, E. Dijkers, A.C. Roldaan, D. Cheung, E.H. Bel, P.J. Sterk, Exhaled breath profiling enables discrimination of chronic obstructive pulmonary disease and asthma, Am. J. Respir. Crit. Care Med. 180 (2009) 1076–1082, https://doi.org/10.1164/rccm.200906-0939OC.

[115] A. McWilliams, P. Beigi, A. Srinidhi, S. Lam, C.E. MacAulay, Sex and smoking status effects on the early detection of early lung cancer in high-risk smokers using an electronic nose, IEEE Trans. Biomed. Eng. 62 (2015) 2044–2054, https://doi.org/10.1109/TBME.2015.2409092.

[116] R. Fernandez-Crehuet, C. Diaz-Molina, J. de Irala, D. Martinez-Concha, I. Salcedo-Leal, J. Masa-Calles, Nosocomial infection in an intensive-care unit identification of risk factors, Infect. Control Hosp. Epidemiol. 18 (1997) 825–830, https://doi.org/10.1086/647552.

[117] R.M. Schnabel, M.L.L. Boumans, A. Smolinska, E.E. Stobberingh, R. Kaufmann, P.M.H.J. Roekaerts, D.C.J.J. Bergmans, Electronic nose analysis of exhaled breath to diagnose ventilator-associated pneumonia, Respir. Res. 109 (2015) 1454–1459, https://doi.org/10.1016/j.rmed.2015.09.014.

[118] Y.-H. Liao, C.-H. Shih, M.F. Abbod, J.-S. Shieh, Y.-J. Hsiao, Development of an E-nose system using machine learning methods to predict ventilator-associated pneumonia, Microsyst. Technol. 28 (2022) 341–351, https://doi.org/10.1007/s00542-020-04782-0.

[119] E.I. Mohamed, M.A. Mohamed, M.H. Moustafa, S.M. Abdel-Mageed, A.M. Moro, A.I. Baess, S.M. El-Kholy, Qualitative analysis of biological tuberculosis samples by an electronic nose-based artificial neural network, Int J Tuberc Lung Dis 21 (2017) 810–817, https://doi.org/10.5588/ijtld.16.0677.

[120] R. Coronel Teixeira, M. Rodríguez, N. Jiménez de Romero, M. Bruins, R. Gómez, J.B. Yntema, G. Chaparro Abente, J.W. Gerritsen, W. Wiegerinck, D. Pérez Bejerano, C. Magis-Escurra, The potential of a portable, point-of-care electronic nose to diagnose tuberculosis, J. Infect. 75 (2017) 441–447, https://doi.org/10.1016/j.jinf.2017.08.003.

[121] R. Coronel Teixeira, D. Ijdema, C. Gómez, D. Arce, M. Roman, Y. Quintana, F. González, N. Jiménez de Romero, D. Pérez Bejarano, S. Aguirre, C. Magis-Escurra, The electronic nose as a rule-out test for tuberculosis in an indigenous population, J. Intern. Med. 290 (2021) 386–391, https://doi.org/10.1111/joim.13281.

[122] H. Hendrick, R. Hidayat, G.J. Horng, Z.H. Wang, Non-invasive method for tuberculosis exhaled breath classification using electronic nose, IEEE Sensor. J. 21 (2021) 11184–11191, https://doi.org/10.1109/JSEN.2021.3061616.